Critical aging and relaxation dynamics in long-range systems

Valerio Pagni [1,*] Friederike Ihssen [2] and Nicolò Defenu [1]

[1] *Institut für Theoretische Physik, ETH Zürich, Wolfgang-Pauli-Strasse 27, 8093 Zürich, Switzerland*

[2] *Institut für Theoretische Physik, Universität Heidelberg, Philosophenweg 16, 69120 Heidelberg, Germany*

(Received 7 January 2026; accepted 14 October 2026; published 9 November 2026)

We study the dynamical scaling of long-range O(N) models after a sudden quench to the critical temperature, using the functional renormalization group approach. We characterize both short-time aging and long-time relaxation as a function of the symmetry index N, the interaction range decay exponent σ, and the dimension d. Our results substantially improve on perturbative predictions, as demonstrated by benchmarks against Monte Carlo simulations and the large-N limit. Finally, we demonstrate that long-range systems increase the performance of critical heat engines with respect to a local active medium.

DOI: 10.1103/31g2-slsh

I. INTRODUCTION

The study of long-range (LR) interacting systems has recently garnered renewed interest due to their relevance in nonequilibrium statistical mechanics [1] and quantum many-body physics [2,3], as well as their experimental realizations in Rydberg atoms, trapped-ion systems, and cold atoms in cavities [2,4–7]. In this work, we focus specifically on the critical dynamics of long-range N-vector spin models—systems in which two-body ferromagnetic interactions decay as a power law, $r^{-(d+\sigma)}$, with the distance r between two classical spins. Here, d denotes the spatial dimension, while σ controls the interaction decay rate.

Consider the dynamics without conservation laws [8] of such a spin system that follows a sudden quench of the temperature from the deeply disordered phase to the critical point—for quenches below the critical temperature (see, e.g., Ref. [9]). While the system undergoes the standard critical relaxation toward equilibrium according to the dynamical exponent z (cf. Ref. [8]) in the long-time limit, the dynamics of correlation functions at shorter times exhibits distinctive nonequilibrium features [10–14], which we refer to as *critical aging*. In general, aging behavior is a hallmark of systems with slow, nonequilibrium dynamics, where physical properties evolve in a history-dependent manner. In contrast to systems featuring a quick relaxation to equilibrium, aging systems display a nontrivial evolution of their correlation and response functions, characterized by a lack of time-translation invariance [15,16]. This phenomenon is observed in a variety of systems, including glassy materials and spin systems [17].

In the context of ferromagnetic spin models, aging in the short-time dynamics is characterized by a nonequilibrium critical exponent θ, which has been extensively studied for short-range (SR) interacting systems [13]. On the other hand, considering their much less investigated long-range counterparts provides two key advantages: control over the critical exponents and a tunable time window during which the characteristic aging properties of the dynamics can be observed. Specifically, the aging exponent θ depends continuously on the decay parameter σ, which interpolates between mean-field (small σ) and short-range (large σ) behaviors [2]. Likewise, the crossover time t_{cross}, marking the transition from short-time behavior to long-time relaxation, can be adjusted accordingly.

Our contribution is threefold: (1) By means of the nonperturbative renormalization group (RG), we characterize the dynamical universality in the whole range of the power-law parameter $\sigma \in (0, \infty)$, overcoming several limitations of the perturbative RG approach of Chen *et al.* [12]. The calculation of the critical exponents z and θ is carried out for several values of N, the number of components of the spins. The Monte Carlo (MC) simulations of the one-dimensional (1D) long-range Ising model [18,19] represent a benchmark for the accuracy of our results for $N = 1$. (2) The existence of an effective fractional dimension D that enables the reconstruction of the *equilibrium* critical properties of the long-range models from a corresponding local model in dimension D has been explored in Refs. [20–24]. In the present work, we extend this framework to *out-of-equilibrium* critical behavior, by providing a dictionary between short- and long-range values of the exponents z and θ. (3) Following the suggestion of Campisi and Fazio [25] of using critical systems as the working medium of a thermodynamic heat engine, we extend this proposal to long-range systems. In this case, through the calculation of what we dub "performance-rate exponent" $\pi_{\text{th}} = \alpha - z\nu$, where α and ν are equilibrium critical exponents, we observe a thermodynamic advantage in the scaling of the performance rate, defined below, over the case with nearest-neighbor interactions.

The paper is structured as follows: In Sec. II, we introduce the model and the temperature quench, including a discussion of the exactly solvable large-N limit. In Sec. III, we present the

*Contact author: vpagni@phys.ethz.ch

Published by the American Physical Society under the terms of the Creative Commons Attribution 4.0 International license. Further distribution of this work must maintain attribution to the author(s) and the published article's title, journal citation, and DOI.

effective dimension approach and its proposed extension to nonequilibrium scenarios. In Sec. IV, we describe the functional renormalization group (fRG) approach that enables us to calculate the dynamical exponent z and the aging exponent θ. Our main results—including those of the performance rate scaling—are presented in Sec. V, followed by the conclusion and outlook in Sec. VI.

II. TEMPERATURE QUENCH OF THE LONG-RANGE O(N) MODELS

We consider a long-range lattice model given by the O(N)-symmetric classical Hamiltonian [2]

$$H = -\frac{1}{2}\sum_{i,j} J_{ij}\boldsymbol{S}_i \cdot \boldsymbol{S}_j, \quad J_{ij} \propto \frac{1}{|i-j|^{d+\sigma}}, \tag{1}$$

where the non-negative matrix elements J_{ij} decay algebraically with the distance between the sites i and j, d is the spatial dimension, $\sigma > 0$ parametrizes the range of the interactions, and $\boldsymbol{S}_i$ are N-component vectors of unit length.

The system is initially prepared in a high-temperature disordered configuration with a nonvanishing but small magnetization M_0. This state is well described by mean-field theory, as critical fluctuations are absent. Then, at time $t = t_0$, the system is suddenly brought to its critical temperature T_c, in the absence of any external magnetic fields. As in the short-range case [10,11,13], we expect to observe some dynamics that depend on microscopic details of the system and of the initial state very shortly after the quench, until a universal behavior emerges at intermediate—but macroscopically *short*—times (see also Ref. [12]). The latter short-time universality manifests itself as critical aging in two-point functions, e.g., the response function:

$$G^R(\boldsymbol{q}, t, t') \sim (t/t')^{\theta} f_R(q(t-t')^{1/z}, t'/t), \quad t' \to t_0, \tag{2}$$

where f_R is a scaling function and θ is the aging exponent [13,14], which is independent of the equilibrium critical exponent for the dynamics we are interested in (i.e., model A, as explained later). Alternatively, one can look at the initial buildup in the magnetization $M(t)$, intuitively explained [11] by noticing that the target temperature of the quench, T_c, is lower than the mean-field critical temperature $T_c^{\rm mf}$, and therefore there is an initial ordering of the spins until a time $\sim t_{\rm cross}$ at which critical correlations have been established. The behavior of magnetization is

$$M(t) = M_0 t^{\theta'} f_M(M_0 t^{\theta'+\beta/(\nu z)}), \tag{3}$$

where $\theta' = \theta + (\sigma - z)/z$—this relation being the generalization of the short-range one [10]—is called initial-slip exponent, and the corresponding scaling function behaves as $f_M(0) = 1$ and $f_M(u \to \infty) \sim u^{-1}$. The exponents β and ν are related to the magnetization and correlation length ξ at equilibrium. As a consequence of the scaling (3), we can estimate the crossover time to be given by $t_{\rm cross} \propto M_0^{-\psi}$, where $\psi = [\theta' + \beta/(\nu z)]^{-1}$. In the long-time limit, the evolution of the system eventually crosses over to the close-to-equilibrium critical dynamics characterized by the divergence of the relaxation time $\tau_{\rm relax} \sim \xi^z$, where z is the dynamical exponent.

In the limit $\sigma \to \infty$ of the Hamiltonian (1), we retrieve the usual nearest-neighbor short-range O(N) vector model. In fact, the same *equilibrium* critical behavior as the short-range model is already recovered for $\sigma \geqslant \sigma_* = 2 - \eta_{\rm SR}$, where $\eta_{\rm SR}$ is the anomalous dimension of the corresponding short-range model. On the other hand, when $0 < \sigma \leqslant \sigma_{\rm mf} = d/2$ the range of interactions is so large that mean-field critical behavior is recovered. The remaining interval $\sigma \in (\sigma_{\rm mf}, \sigma_*)$ exhibits genuine long-range critical behavior, where the critical exponents are a continuous function of the parameter σ [2]. The universal properties of the Hamiltonian (1) correspond to those of the effective field theory

$$\mathcal{H}[\boldsymbol{\varphi}] = \int_{\boldsymbol{x}} \left\{ \frac{1}{2}\left(\nabla^{\frac{\sigma}{2}}\boldsymbol{\varphi}\right)^2 + \frac{\tau}{2}\boldsymbol{\varphi}^2 + \frac{g}{4!}(\boldsymbol{\varphi}^2)^2 \right\}, \tag{4}$$

where $\int_{\boldsymbol{x}} \equiv \int d^d\boldsymbol{x}$ and $\boldsymbol{\varphi} = (\varphi_1, \ldots, \varphi_N)$ is a continuous field. In the infrared, the fractional gradient can be interpreted in momentum space as follows: $\int_{\boldsymbol{x}} (\nabla^{\frac{\sigma}{2}}\boldsymbol{\varphi}(\boldsymbol{x}))^2 = \int_{\boldsymbol{q}} q^{\sigma}\boldsymbol{\varphi}(-\boldsymbol{q}) \cdot \boldsymbol{\varphi}(\boldsymbol{q})$, where $\int_{\boldsymbol{q}} \equiv (2\pi)^{-d}\int d^d q$ and $\boldsymbol{\varphi}(\boldsymbol{q})$ is the Fourier transform of $\boldsymbol{\varphi}(\boldsymbol{x})$. At tree level, the relevance of long-range couplings in the low-energy limit is obtained by comparing the scaling dimension of the fractional gradient k^{σ} with the one of the conventional local gradient term k^2, where k is the infrared cutoff scale. The boundary $\sigma_* = 2 - \eta_{\rm SR}$ is obtained by comparing the scaling dimension of the long-range operator with the one of the renormalized local kinetic term $k^{2-\eta_{\rm SR}}$, as first argued by J. Sak [26].

Sak's crossover scenario has been thoroughly investigated over the years, with many studies focusing on the Ising model ($N = 1$): References [27,28] predict the crossover to remain at $\sigma^* = 2$ even for the full theory, but this finding has been attributed to the difficulty of capturing logarithmic corrections close to the boundary [21]. Sak's picture is confirmed by MC simulations in two dimensions (2D) [21,29] and RG approaches [22,30]. Conformal perturbation theory studies agree with Sak's criterion in both two and three dimensions [31,32]. More recently, interest has been shifted to $d = 1$, where the crossover at $\sigma^* = 1$ has been investigated by both conformal perturbation theory [33] and functional RG [34].

In the same spirit, we set out to study the critical dynamics of the system from a field-theoretical perspective. In particular, we investigate the above scenario applied to critical behavior of long-range systems away from thermal equilibrium. We remark that the dynamics we are considering is not directly given by the Hamiltonian (1). Rather, it is implemented phenomenologically at the mesoscopic level by requiring that the system relaxes to a Gibbs distribution and that possible conservation laws are retained by constraining the ensemble [8,35]. We work in the absence of any conservation laws; i.e., we take into account the dynamics of model A in the traditional classification [8]. Therefore, one writes a Langevin equation of the form

$$\partial_t \varphi(t, \boldsymbol{x}) = -\mathcal{D}\frac{\delta\mathcal{H}[\varphi]}{\delta\varphi(t, \boldsymbol{x})} + \zeta(t, \boldsymbol{x}), \tag{5}$$

where $\mathcal{D}$ is a constant relaxation rate and ζ is a zero-mean Markovian and Gaussian noise with correlation

$$\langle \zeta(t_1, \boldsymbol{x}_1)\zeta(t_2, \boldsymbol{x}_2)\rangle = 2\Omega\,\delta(\boldsymbol{x}_1 - \boldsymbol{x}_2)\delta(t_1 - t_2). \tag{6}$$

The Einstein relation [36] is realized when the amplitude of the noise is $\Omega = \mathcal{D}$ (working in units where $k_B T = 1$). Instead of computing observables such as magnetization $\boldsymbol{M}(t) = \langle \boldsymbol{\varphi}(t) \rangle$ by averaging over solutions to the stochastic equation (5), one can recast the problem in terms of functional integrals, by means of the Martin-Siggia-Rose-Janssen-de Dominicis (MSRJD) [37–39] or response field formalism, where auxiliary (response) fields $\tilde{\boldsymbol{\varphi}}$ are introduced for each component of the order-parameter field $\boldsymbol{\varphi}$. Importantly, information about the initial state has to be taken into account in our analysis. This procedure leads to a field-theoretical problem described by the action [10,11,13]

$$S[\varphi, \tilde{\varphi}] = \int_{\boldsymbol{x}} \frac{\tau_0}{2} [\boldsymbol{\varphi}_0(\boldsymbol{x}) - \boldsymbol{h}(\boldsymbol{x})]^2 + \int_{t>t_0} \int_{\boldsymbol{x}} \left\{ \tilde{\varphi}_i \partial_t \varphi_i + \mathcal{D} \tilde{\varphi}_i \frac{\delta \mathcal{H}[\boldsymbol{\varphi}]}{\delta \varphi_i} - \tilde{\varphi}_i \Omega \tilde{\varphi}_i \right\}, \quad (7)$$

where summation over repeated indices is implied, $\int_{t>t_0} \equiv \int_{t_0}^{\infty} dt$, and the first line encodes the Gaussian probability distribution of the initial high-temperature state $\boldsymbol{\varphi}_0(\boldsymbol{x}) \equiv \boldsymbol{\varphi}(t_0, \boldsymbol{x})$ with

$$\langle \boldsymbol{\varphi}_0(\boldsymbol{x}) \rangle = \boldsymbol{h}(\boldsymbol{x}),$$
$$\langle [\boldsymbol{\varphi}_0(\boldsymbol{x}) - \boldsymbol{h}(\boldsymbol{x})][\boldsymbol{\varphi}_0(\boldsymbol{x}') - \boldsymbol{h}(\boldsymbol{x}')] \rangle = \tau_0^{-1} \delta(\boldsymbol{x} - \boldsymbol{x}'). \quad (8)$$

Given that the field φ—as well as φ_0—has mass dimension $(d - \sigma)/2$, one finds that the dimension of τ_0 is $\sigma > 0$. Hence, under renormalization, $(\tau_0^{-1})^* = 0$ is the only fixed-point value of the initial correlation length compatible with the normalization of the probability distribution.

Thus, the scaling forms (2) and (3) can be obtained by an RG analysis similar to those of Refs. [10,11,13]. In particular, from a field-theoretical point of view, a new exponent θ (or θ') arises due to the fact that the response field at the initial time surface, $\tilde{\boldsymbol{\varphi}}_0 = \tilde{\boldsymbol{\varphi}}(t = t_0)$, has to be renormalized independently of the "bulk" fields and therefore it acquires an anomalous dimension $\tilde{\eta}_0$ (see Sec. IV).

Before considering the strongly interacting critical model, it is convenient to inspect the quadratic model obtained by setting $g = 0$ in Eq. (4). In this case, the correlation and response functions—defined as $G^C_{0,ij}(\boldsymbol{q}, t, t') \equiv \langle \varphi_i(\boldsymbol{q}, t) \varphi_j(-\boldsymbol{q}, t') \rangle_0 = \delta_{ij} G^C_0(\boldsymbol{q}, t, t')$ and $G^R_{0,ij}(\boldsymbol{q}, t, t') \equiv \langle \varphi_i(\boldsymbol{q}, t) \tilde{\varphi}_j(-\boldsymbol{q}, t') \rangle_0 = \delta_{ij} G^R_0(\boldsymbol{q}, t, t')$ (see, e.g., Ref. [36])—read

$$G^C_0(\boldsymbol{q}, t, t') = \frac{1}{\omega_q} \left[e^{-\omega_q |t - t'|} + \left(\frac{\omega_q}{\tau_0} - 1 \right) e^{-\omega_q (t + t' - 2t_0)} \right], \quad (9a)$$

$$G^R_0(\boldsymbol{q}, t, t') = \vartheta(t - t') e^{-\omega_q (t - t')}, \quad (9b)$$

where $\vartheta(\cdot)$ is the Heaviside step function, the dispersion relation ω_q (with $q = |\boldsymbol{q}|$) is

$$\omega_q = q^\sigma + \tau, \quad (10)$$

and we have set $\Omega = \mathcal{D} = 1$. Comparing Eq. (2) with Eq. (9b), we obtain $\theta_{\rm mf} = 0$ as the mean-field value of the aging exponent. Similarly, $z_{\rm mf} = \sigma$, so that $\theta'_{\rm mf} = 0$ as well. Hence, it is apparent that critical aging is a genuinely collective phenomenon that requires a non-mean-field description.

A first step toward that is provided by the large-N limit, where the number of field components is taken to be infinite. In fact, following Refs. [10,40], we can decouple self-consistently the nonlinearity in the action (4). This is exact as $N \to \infty$, in which case fluctuations of the variable $N^{-1} \boldsymbol{\varphi}^2 = N^{-1} \sum_i \varphi_i^2$ are strongly suppressed (see, e.g., Ref. [41]). More precisely, after a rescaling of g by a factor of N, we make the replacement

$$\frac{g}{N} \sum_{i,j=1}^{N} \tilde{\varphi}_i \varphi_i \varphi_j \varphi_j \to g C(t) \sum_{i=1}^{N} \tilde{\varphi}_i \varphi_i, \quad (11)$$

where

$$C(t) \equiv G^C(\boldsymbol{0}, t, t) = \frac{1}{N} \sum_{i=1}^{N} \langle \varphi_i(\boldsymbol{x}, t) \varphi_i(\boldsymbol{x}, t) \rangle = \int_{\boldsymbol{q}} C(\boldsymbol{q}, t), \quad (12)$$

is the equal-time correlator. The resulting action is quadratic in the fields, where, however, the quadratic coupling has become time dependent:

$$\tau \to \tau + \frac{g}{6} C(t) \equiv \tau_C(t). \quad (13)$$

It turns out, as detailed in Appendix A, that the scaling behavior of the response function is

$$G^R(\boldsymbol{q}, t, t') = \vartheta(t - t') (t/t')^\theta e^{-q^\sigma (t - t')}, \quad (14)$$

with an aging exponent

$$\theta = 1 - \frac{d}{2\sigma}, \quad (15)$$

which represents an important benchmark for Sec. V in order to test the fRG for O(N) models with $N \gg 1$. Moreover, comparing Eq. (14) with Eq. (2), we also note that $z = \sigma$ in the large-N limit. As announced, this result already shows that θ and z can be tuned by changing the range σ of the interactions. Notice that Eq. (15) can be compared with the large-N estimate of the short-range counterpart of the aging exponent, which reads $\theta_{\rm SR} = 1 - D/4$ for a D-dimensional short-range model [10]. The exponents match exactly if $D = 2d/\sigma$, where d is the dimension of the *long*-range system. In the following, we explore this equivalence in greater detail and beyond the large-N limit.

III. EFFECTIVE DIMENSION APPROACH

In thermal equilibrium, the effective dimension approach [20–24] enables us to obtain a pretty accurate (yet not exact) idea of the critical behavior of a long-range model in dimension d with decay exponent σ by looking at the corresponding results obtained for a short-range system in the fractional dimension $D = D(\sigma)$. In this section, we briefly review this dimensional correspondence and extend it to out-of-equilibrium systems.

Rather than looking at the free energy density as in Refs. [20,21,24], we prefer to work directly with correlation functions, in order to more clearly reveal the connection with

dynamics, where the generating functional obtained from Eq. (7) in the MSRJD framework has a less transparent physical meaning than the equilibrium partition function.

It is well known from the usual real-space RG applied to finite-size systems (see, e.g., Refs. [35,42]) that the two-point response function for a nearly critical macroscopic system with $\mathcal{N} = L^d$ spins in the bulk obeys

$$G(r, t; \{u_\alpha\}) = L^{2(y_h - d)} G(L^{-1} r, L^{-z} t; \{u'_\alpha\}), \tag{16}$$

after a suitable number of RG iterations. Here, $\{u_\alpha\}$ indicate the couplings of the model, among which the relevant ones are the reduced temperature τ and magnetic field h, while $u'_\alpha = L^{y_\alpha} u_\alpha$ are the couplings rescaled according to their RG eigenvalues y_α. The relevant couplings have positive eigenvalues y_τ and y_h, related to the critical exponents ν and η by $\nu = 1/y_\tau$ and $\eta = d + 2 - 2y_h$. The dynamical exponent z quantifies the anisotropy between spatial and temporal directions.

The idea of the effective dimension approach is to compare the scaling of the response function between a long-range model and a short-range model with the same number of spins $\mathcal{N} = L^d = L_{\rm SR}^D$. Hereafter, the quantities of the short-range model will be denoted by the label "SR", except $d_{\rm SR} \equiv D$. Thus, equating the right-hand side of Eq. (16) at criticality for the long-range and short-range models yields

$$\frac{2 - \eta(\sigma)}{d} = \frac{2 - \eta_{\rm SR}(D)}{D}, \tag{17}$$

$$\frac{z(\sigma)}{d} = \frac{z_{\rm SR}(D)}{D}. \tag{18}$$

Before discussing how to obtain the effective dimension $D = D(\sigma)$ of the short-range system, we notice that Eq. (18) is already a result pertaining dynamics, even though limited to relaxation close to equilibrium at long times.

In fact, to obtain the effective dimension, one needs the additional information that in the long-range case interactions cannot renormalize the nonanalytic kinetic term; thus, $\eta(\sigma) = 2 - \sigma$ even beyond mean-field theory [26,43,44]. Then, using Eq. (17), we obtain that the effective dimension $D = D(\sigma)$ of the SR system is

$$D = \frac{2 - \eta_{\rm SR}(D)}{\sigma} d. \tag{19}$$

This is an implicit equation, because one needs to know the value of the critical exponent $\eta_{\rm SR}$ in fractional dimensions (see, e.g., Ref. [45]) to calculate D, as discussed further in Sec. V.

Finally, replacing expression (16) with the analogous nonequilibrium form of the correlation and response functions given in Refs. [10,13] [see also Eq. (14)], we are able to confirm the effective dimension relation between long- and short-range models for the aging exponent. In particular, considering the two-time dependence $(t/t')^\theta$,

$$\theta(\sigma) = \theta_{\rm SR}(D(\sigma)). \tag{20}$$

This generalizes the discussion in the last paragraph of Sec. II to the case where N is finite and, accordingly, the anomalous dimension $\eta_{\rm SR}(D)$ appearing in Eq. (19) is nonvanishing.

We stress again that, as discussed in Refs. [20–24,32], the correspondence between short- and long-range models via the effective dimension is not exact. However, for the two-dimensional long-range Ising model, Ref. [24] tested the effective dimension prediction for the correlation-length exponent against conformal-bootstrap (CB) data and found agreement better than 97% over the whole parameter range. In the following, we investigate its extension to out-of-equilibrium criticality in two complementary ways. First, in Sec. V, we compare long-range and short-range calculations performed independently within the same fRG truncation, in order to test whether the effective dimension correspondence is preserved by our approximation. Second, in Sec. V A, we apply the correspondence to Monte Carlo estimates for short-range models and compare the resulting predictions with long-range Monte Carlo data, thereby providing a benchmark that does not rely on field-theoretical descriptions.

IV. RENORMALIZATION GROUP

In order to obtain the dynamical scaling properties of the long-range model captured by the action (7), we use the functional and nonperturbative RG approach reviewed in Refs. [46,47]. These two features allow us to compute results for the whole range of values of the decay parameter σ and number N of components of the field. A unified fRG treatment has been already carried out for both classical and quantum long-range O(N) models in equilibrium [48]. In Sec. IV A, we introduce our nonequilibrium fRG setup, combining the Wetterich equation with the MSRJD description of critical dynamics with a time boundary [14,49]. The scaling of the quantities that undergo renormalization, resulting in a definition of the exponents z and θ, is described in Sec. IV B. The propagators and the projection scheme used to derive the flow equations are presented in Sec. IV C. Finally, in Sec. IV D, we report the resulting flow equations and expressions for the dynamical critical exponents.

A. Nonequilibrium fRG

Let us introduce a mass scale $k \in [0, \Lambda]$, where Λ is a UV cutoff proportional to the inverse of the lattice spacing of Eq. (1). In the fRG framework, we attach a k dependence to the generating functional obtained from Eq. (7) and related quantities via the introduction of a regulator $\mathbb{R}_k$ that suppresses the propagation of low-energy modes. In particular, instead of Eq. (7), one considers a description in terms of a 1PI effective average action $\Gamma_k = \Gamma_k[\boldsymbol{\phi}, \tilde{\boldsymbol{\phi}}]$, which interpolates between the bare action $\Gamma_\Lambda = S$ and the (unknown) genuine effective action $\Gamma_0 = \Gamma$ as the scale k is lowered. The scale dependence of the effective action is captured by the Wetterich equation [46,47,50], which in our nonequilibrium case ($t > t_0$) reads [14,49]

$$\partial_\kappa \Gamma_k[\boldsymbol{\Phi}] = \frac{1}{2} \int_{\boldsymbol{x}, t > t_0} \mathrm{tr}[\mathbb{G}_k[\boldsymbol{\Phi}](t, \boldsymbol{x}; t, \boldsymbol{x}) (\partial_\kappa \mathbb{R}_k)], \tag{21}$$

where $\kappa = \ln(k/\Lambda)$ is the RG time, $\boldsymbol{\Phi} = (\boldsymbol{\phi}, \tilde{\boldsymbol{\phi}})$ is the "superfield", the trace is over N-vector components and the 2×2 superfield structure, and

$$\mathbb{G}_k[\boldsymbol{\Phi}] = \left(\Gamma_k^{(2)}[\boldsymbol{\Phi}] + \mathbb{R}_k\right)^{-1} \tag{22}$$

is the full field-dependent propagator. The regulator matrix $\mathbb{R}_k$ is chosen diagonal in the O(N)-components, while it is purely off-diagonal in $(\boldsymbol{\phi}, \tilde{\boldsymbol{\phi}})$ space [47,51,52]. This means that we have a $2N \times 2N$ block diagonal matrix, which takes the following form in momentum space:

$$\mathbb{R}_{k,ij}(q^\sigma) = \delta_{ij}\hat{\tau}_1 R_k(q^\sigma), \quad \hat{\tau}_1 = \begin{pmatrix} 0 & 1 \\ 1 & 0 \end{pmatrix}, \tag{23}$$

where R_k—specified later—is assumed to be independent of time, although this may be improved as in Ref. [53].

As usual, Eq. (21) being a functional integro-differential equation, the only possibility to proceed is to specify some ansatz for the form of the effective action. On the basis of the bare action (7), a sensible choice is [14,49]

$$\begin{aligned}\Gamma_k = &\int_{\boldsymbol{x}} \left[-\frac{Z_{0,k}^2}{2\tau_0}\tilde{\phi}_{0,i}(\boldsymbol{x})^2 + Z_{0,k}\tilde{\phi}_{0,i}(\boldsymbol{x})\phi_{0,i}(\boldsymbol{x}) \right] \\ &+ \int_{\boldsymbol{x},t>t_0} \tilde{\phi}_i(t,\boldsymbol{x})[(Z_k\partial_t + K_k\nabla^\sigma)\phi_i(t,\boldsymbol{x}) - \Omega_k\tilde{\phi}_i(t,\boldsymbol{x})] \\ &+ \int_{\boldsymbol{x},t>t_0} \tilde{\phi}_i(t,\boldsymbol{x})V_k^{(i)}(\boldsymbol{\phi}(t,\boldsymbol{x})),\end{aligned} \tag{24}$$

where we have introduced the (field-independent) renormalization functions $Z_{0,k}$, Z_k, K_k, Ω_k and the fully field-dependent effective potential $V_k(\boldsymbol{\phi})$. No independent boundary renormalization is assigned to ϕ_0. Indeed, at the initial-condition fixed point $\tau_0^{-1} = 0$, its fluctuations vanish [see Eq. (8)]. The leading nontrivial order-parameter operator at the initial-time surface is instead $\partial_t\phi|_{t=t_0}$, which causality relates to $\tilde{\phi}_0$ [10,11]. Their boundary singularities are therefore absorbed by the single additional renormalization function $Z_{0,k}$ associated with $\tilde{\phi}_0$.

B. Dimensional analysis

In order to uncover the fixed-point solutions associated with the flows obtained from Eq. (21) (cf. Sec. IV D), we need to first adimensionalize the quantities entering the effective action (24), which is itself dimensionless, $[\Gamma_k] = 0$. Scaling dimensions $[\cdot]$ are defined in terms of the external scale k.

Since space and time scale anisotropically according to the dynamical critical exponent z, we consider the scaling dimension of a spatial coordinate to be $[x] = -1$, while for time $[t] = -z$. Also, we assume the typical scaling $K_k \sim k^{-\eta_K}$ of the wavefunction renormalization as $k \to 0$, where η_K is the anomalous dimension. Hence, $[K_k] = -\eta_K$, and similarly $[Z_k] = -\eta_Z$ for some η_Z that we will determine from the flow of Z_k as $\eta_Z = -\partial_\kappa \ln Z_k$. From these general assumptions, it follows directly that the dimensional consistency of $Z\partial_t + K\nabla^\sigma$ implies

$$z = \sigma + \eta_Z - \eta_K, \tag{25}$$

where it is known that $\eta_K = 0$ for the LR model [48]. In the absence of quantum corrections, we deduce from Eq. (25) that the mean-field result is $z_{\rm mf} = \sigma$, as anticipated. Dimensional considerations on the quadratic part of the bulk action lead to $[\phi] + [\tilde{\phi}] = d - \sigma + \eta_K + z$. Taking the dimension of ϕ to be the same as in equilibrium yields

$$[\phi] = \frac{d - \sigma + \eta_K}{2} \quad \text{and} \quad [\tilde{\phi}] = [\phi] + z. \tag{26}$$

Moreover, if $[\Omega_k] = -\eta_\Omega$, from Eqs. (25) and (26) we find that $\eta_\Omega = \eta_Z$. All of this is consistent with the last line of Eq. (24) provided $[V_k] = d$, the usual dimension of the effective potential. We conclude that the dimensionless and renormalized quantities to be used later are

$$\begin{aligned}&\bar{x} = kx, \quad \bar{t} = k^z t, \\ &\bar{\rho}(\bar{t},\bar{\boldsymbol{x}}) \equiv K_k k^{\sigma-d}\rho(t,\boldsymbol{x}), \quad u_k(\bar{\rho}) \equiv k^{-d}U_k(\rho).\end{aligned} \tag{27}$$

Let us finally consider the dimensions of the boundary action. Since $\tilde{\phi}_0$ alone is responsible for the introduction of a novel boundary exponent [10,11,13], we take $\phi_0 = \phi(t=0)$ to have the same dimension as ϕ, i.e., $[\phi_0] = [\phi]$. Assuming the scaling $Z_{0,k} \sim k^{-\eta_{Z_0}}$ in the infrared limit $k \to 0$, from the first line of Eq. (24) we find

$$[\tilde{\phi}_0] = [\tilde{\phi}] + \eta_{Z_0} - \eta_Z \quad \text{and} \quad [\tau_0] = \sigma - \eta_K. \tag{28}$$

In the absence of anomalous scaling, the dimension of $\tilde{\phi}_0$ would be the same as that of the bulk response field $\tilde{\phi}$. However, in general, such anomalous scaling is related to the aging exponent θ via [10,13]

$$\theta = \frac{\eta_Z - \eta_{Z_0}}{z}. \tag{29}$$

C. Propagators and projection scheme

The derivation of the flow equations requires three main steps. We first evaluate $\Gamma_k^{(2)} + \mathbb{R}_k$ on a spatially uniform background and invert it to obtain the correlation and response functions. We then take suitable field derivatives of the Wetterich equation (21) and project the resulting vertex functions onto the field, momentum, frequency, and initial-time structures retained in ansatz (24). In the following, we outline this procedure, while the details are presented in Appendixes B–D.

The O(N) symmetry implies that the effective potential depends on the order-parameter field only through the invariant $\rho = \boldsymbol{\phi}^2/2$, so that we write $V_k(\boldsymbol{\phi}) = U_k(\rho)$. Its field derivatives are denoted by

$$\begin{aligned}&\partial_{\phi_i} V_k \equiv V_k^{(i)} = \phi_i U_k'(\rho), \\ &\partial_{\phi_i}\partial_{\phi_j} V_k \equiv V_k^{(ij)} = \delta_{ij}U_k'(\rho) + \phi_i\phi_j U_k''(\rho),\end{aligned} \tag{30}$$

and analogously for higher derivatives.

To evaluate the Hessian and the vertex functions, we expand around a spatially uniform background,

$$\boldsymbol{\phi}_*(t) = \boldsymbol{\phi}_u + \delta\boldsymbol{\phi}(t), \quad \boldsymbol{\phi}_u = (\sqrt{2\rho}, 0, \ldots, 0), \tag{31a}$$

$$\tilde{\boldsymbol{\phi}}_*(t) = \tilde{\boldsymbol{\phi}}_u + \delta\tilde{\boldsymbol{\phi}}(t), \quad \tilde{\boldsymbol{\phi}}_u = \boldsymbol{0}. \tag{31b}$$

The orientation of $\boldsymbol{\phi}_u$ is chosen without loss of generality by virtue of the O(N) symmetry, while the auxiliary response field vanishes on the physical background in the absence of external sources [52]. For the bulk projections, the time-dependent corrections can be neglected and the expansion is performed around the stationary configuration $\boldsymbol{\Phi}_u = (\boldsymbol{\phi}_u, \boldsymbol{0})$. They must instead be retained when extracting contributions localized at the initial-time surface. After taking the required

functional derivatives, we evaluate the resulting expressions at the running minimum $\rho = \rho_{\min,k}$ of the effective potential, defined by $U_k'(\rho_{\min,k}) = 0$.

On the stationary background $\boldsymbol{\Phi}_u$, the regulated inverse propagator [see Eq. (22)] is diagonal in the O(N) indices. The direction selected by $\boldsymbol{\phi}_u$ defines a longitudinal mode, while the remaining $N-1$ components correspond to transverse modes. Their field-dependent renormalized dispersions are

$$\omega_{L,k}(q^\sigma) = K_k q^\sigma + R_k(q^\sigma) + U_k'(\rho) + 2\rho U_k''(\rho), \quad (32a)$$

$$\omega_{T,k}(q^\sigma) = K_k q^\sigma + R_k(q^\sigma) + U_k'(\rho). \quad (32b)$$

Accordingly, the inversion of $\mathbb{G}_k^{-1}$ reduces to the separate inversion of one longitudinal and $N-1$ identical transverse 2×2 blocks in correlation-response field space.

In the bulk (equivalently, in the limit $t_0 \to -\infty$), time-translation invariance is restored and the regulated Hessian can be inverted in frequency space. Transforming back to the time domain gives, for each sector $i \in \{L, T\}$,

$$\mathbb{G}_{\mathrm{eq},i}(t,t') = \begin{pmatrix} G^C_{\mathrm{eq},i}(t,t') & G^R_{\mathrm{eq},i}(t,t') \\ G^R_{\mathrm{eq},i}(t',t) & 0 \end{pmatrix}, \quad (33)$$

where

$$G^C_{\mathrm{eq},i}(t,t') = \frac{\Omega_k}{Z_k \omega_{i,k}}[e^{-\omega_{i,k}|t-t'|/Z_k}], \quad (34a)$$

$$G^R_{\mathrm{eq},i}(t,t') = \frac{\vartheta(t-t')}{Z_k} e^{-\omega_{i,k}(t-t')/Z_k}. \quad (34b)$$

These time-translation-invariant propagators are used to determine the bulk flows of U_k, K_k, Z_k, and Ω_k. Their explicit derivation is presented in Appendix C. Here and in what follows, the subscript "eq" (for "equilibrium") indicates that the propagator is time-translation invariant, depending on t and t' only through $t-t'$.

To determine the flow of the boundary renormalization function $Z_{0,k}$, the initial time t_0 must instead be kept finite, which breaks time-translation invariance. The correlation function $G^C_{0,i}(t,t') = G^C_{\mathrm{eq},i}(t,t') + G^C_{\mathrm{neq},i}(t,t')$ acquires an additional transient contribution

$$G^C_{\mathrm{neq},i}(t,t') \propto e^{-\omega_{i,k}(t+t'-2t_0)/Z_k}. \quad (35)$$

In contrast, the response function remains unchanged, $G^R_{0,i}(t,t') = G^R_{\mathrm{eq},i}(t,t')$. Although the additional term in Eq. (35) decays exponentially away from the initial-time surface, it must be retained to extract the boundary-localized flow of $Z_{0,k}$. The full expression for its prefactor and the inversion of the Hessian at finite t_0 are given in Appendix C.

Having obtained the propagators, we take suitable field derivatives of the Wetterich equation. Denoting either $\boldsymbol{\phi}$ or $\tilde{\boldsymbol{\phi}}$ collectively by $\boldsymbol{\Phi}$, the variation of the full propagator follows from

$$\delta_{\boldsymbol{\Phi}} \mathbb{G}_k = -\mathbb{G}_k \big(\delta_{\boldsymbol{\Phi}} \Gamma_k^{(2)}\big) \mathbb{G}_k. \quad (36)$$

A second field derivative consequently generates the standard sunset contributions, containing three propagators and two first variations of the Hessian, and a tadpole contribution, containing two propagators and one second variation of the Hessian. Products in these expressions imply integrations over intermediate spacetime arguments and summations over internal indices. The explicit functional variations, including the contributions localized at $t = t_0$, are given in Appendix B.

The running functions are identified by matching the field derivatives of the Wetterich equation with the corresponding structures in ansatz (24). The flow of the potential is obtained from the one-point response-field vertex on the uniform background,

$$\partial_\kappa U_k'(\rho) = \frac{1}{\sqrt{2\rho}} \frac{\delta}{\delta \tilde{\phi}_1} \partial_\kappa \Gamma_k \Big|_{\boldsymbol{\Phi}=\boldsymbol{\Phi}_u}, \quad (37)$$

where vanishing external momentum and frequency are understood. For the remaining bulk functions, we take two derivatives in the transverse sector $i = g \neq 1$ (see the discussion below). Defining the corresponding mixed two-point flow by

$$\partial_\kappa \Gamma^{(2)}_{k,\tilde{\phi}_g \phi_g}(\omega, \boldsymbol{q}) \equiv \frac{\delta^2 \partial_\kappa \Gamma_k}{\delta \tilde{\phi}_g(-\omega, -\boldsymbol{q})\, \delta \phi_g(\omega, \boldsymbol{q})} \Big|_{\boldsymbol{\Phi}=\boldsymbol{\Phi}_u}, \quad (38)$$

the flows of K_k and Z_k are determined by

$$\partial_\kappa K_k = \partial_{q^\sigma} \partial_\kappa \Gamma^{(2)}_{k,\tilde{\phi}_g \phi_g}(0, \boldsymbol{q})|_{\boldsymbol{q}=0}, \quad (39)$$

$$\partial_\kappa Z_k = -i \partial_\omega \partial_\kappa \Gamma^{(2)}_{k,\tilde{\phi}_g \phi_g}(\omega, \boldsymbol{0})|_{\omega=0}. \quad (40)$$

Since the loop corrections do not generate a nonanalytic contribution proportional to q^σ, the first of these projections vanishes, so $\partial_\kappa K_k = 0$. The noise amplitude is obtained from the response-response two-point function,

$$\partial_\kappa \Omega_k = -\frac{1}{2} \frac{\delta^2 \partial_\kappa \Gamma_k}{\delta \tilde{\phi}_g(-\omega, -\boldsymbol{q})\, \delta \tilde{\phi}_g(\omega, \boldsymbol{q})} \Big|_{\substack{\boldsymbol{\Phi}=\boldsymbol{\Phi}_u \\ \omega=0,\ \boldsymbol{q}=0}}. \quad (41)$$

Finally, $Z_{0,k}$ is extracted at finite t_0 by matching the coefficient of the boundary-localized variation $\delta\phi_{0,g}\delta\tilde{\phi}_{0,g}$:

$$\partial_\kappa Z_{0,k}\, \delta\phi_{0,g}\delta\tilde{\phi}_{0,g} = \frac{\delta^2 \partial_\kappa \Gamma_k}{\delta \phi_g\, \delta \tilde{\phi}_g} \Big|_{\boldsymbol{\Phi}=\boldsymbol{\Phi}_u} \Big|_{\delta\phi_{0,g}\delta\tilde{\phi}_{0,g}}. \quad (42)$$

For the bulk projections, we retain the time-translation-invariant part of the propagator and discard the transient contributions, which are exponentially suppressed with the distance from the initial-time surface. The boundary projection is treated separately: The initial time is kept finite and the contribution proportional to $\delta\phi_{0,g}\delta\tilde{\phi}_{0,g}$ is isolated using the short-time expansion described in Appendix F. Applying these projections yields the flow equations and anomalous dimensions summarized in the following subsection, while their explicit evaluation is presented in Appendix D.

D. Flow equations and critical exponents

Applying the projections described above, we obtain the following flow equation for the derivative of the dimensionless effective potential:

$$\begin{aligned} \partial_\kappa u_k'(\overline{\rho}) = {} & (-\sigma + \eta_K) u_k'(\overline{\rho}) + (d - \sigma + \eta_K)\overline{\rho} u_k''(\overline{\rho}) \\ & - \frac{4 v_d}{\sigma} \big[\mu_L'(\overline{\rho}) L_1^{(d,\sigma)}(\mu_L) \\ & + (N-1)\mu_T'(\overline{\rho}) L_1^{(d,\sigma)}(\mu_T)\big], \end{aligned} \quad (43)$$

where $v_d^{-1} = 2^{d+1}\pi^{d/2}\Gamma(d/2)$, the functions $L_n^{(d,\sigma)}$ are described in Appendix E, and the longitudinal and transverse masses are

$$\mu_L(\overline{\rho}) = u_k'(\overline{\rho}) + 2\overline{\rho}u_k''(\overline{\rho}) \quad \text{and} \quad \mu_T(\overline{\rho}) = u_k'(\overline{\rho}). \tag{44}$$

Equation (43) is consistent with static fRG [2,22,48]. The dimensionless form is particularly useful because, instead of studying the full RG flow of the potential, we can focus on its fixed-point value $u_*'(\rho)$, obtained by setting $\partial_\kappa u_k' = 0$ and solving the resulting ordinary differential equation. Physically, this captures precisely the scaling properties relevant to the critical behavior.

For each function $A_k \in \{Z_{0,k}, Z_k, K_k, \Omega_k\}$, we define the corresponding anomalous dimensions $\eta_A \coloneqq -\partial_\kappa \ln A_k$. As mentioned above, K_k does not flow, and therefore $\eta_K = 0$. Moreover, we observe $\eta_\Omega = \eta_Z$, which corroborates *a posteriori* our dimensional analysis. The explicit expressions for η_{Z_0} and $\eta_Z = \eta_\Omega$ are given in Eqs. (D7b) and (D12), respectively. For a generic regulator $R_k(q^\sigma)$, they take the form of momentum integrals involving derivatives of the effective potential. Together, with Eqs. (29) and (25), they determine the dynamical exponents θ and z. From a technical point of view, we obtain Eqs. (D7b) and (D12) upon projecting to one of the transverse components $i \neq 1$, as discussed in Ref. [14].

The present calculation corresponds to the leading iteration of the expansion introduced in Ref. [14]. At this order, the bulk couplings and vertices are obtained from the fully interacting, time-translation invariant fixed-point solution, while the propagator retains the finite-t_0 contribution required for the boundary projection. This already generates an independent flow of $Z_{0,k}$ and hence the nontrivial aging exponent (29). The bulk projections are instead performed onto the time-translation-invariant sector, where detailed balance implies $\eta_\Omega = \eta_Z$ and determines the asymptotic exponent z. Further iterations would retain the explicitly time-dependent corrections generated by the flow and feed them back into the propagator. Promoting Z_k and Ω_k to time-dependent functions would then allow one to capture transient deviations from the equilibrium fluctuation-dissipation relation. Such corrections vanish as the system relaxes toward equilibrium, but may provide quantitative corrections to the finite-time dynamics.

The numerical results for the dynamical exponents in Eqs. (25) and (29) are obtained by substituting the fixed-point $u_*(\overline{\rho})$ of the effective potential and its derivatives evaluated at the minimum $\overline{\rho}_{\min}$. In fact, it is straightforward to make Eqs. (D7b) and (D12) dimensionless, so that at the critical point they exhibit no k dependence, with only the dimensionless potential entering these expressions.

V. RESULTS

In this section, we present the results obtained for the critical exponents θ and z describing the dynamical scaling properties of a long-range model subject to a sudden critical quench at time $t = t_0$. We have obtained the fixed-point potential $u_*(\overline{\rho})$ coming from our fRG analysis by making an explicit regulator choice:

$$R_k(q^\sigma) = K_k(k^\sigma - q^\sigma)\,\theta(k^\sigma - q^\sigma), \tag{45}$$

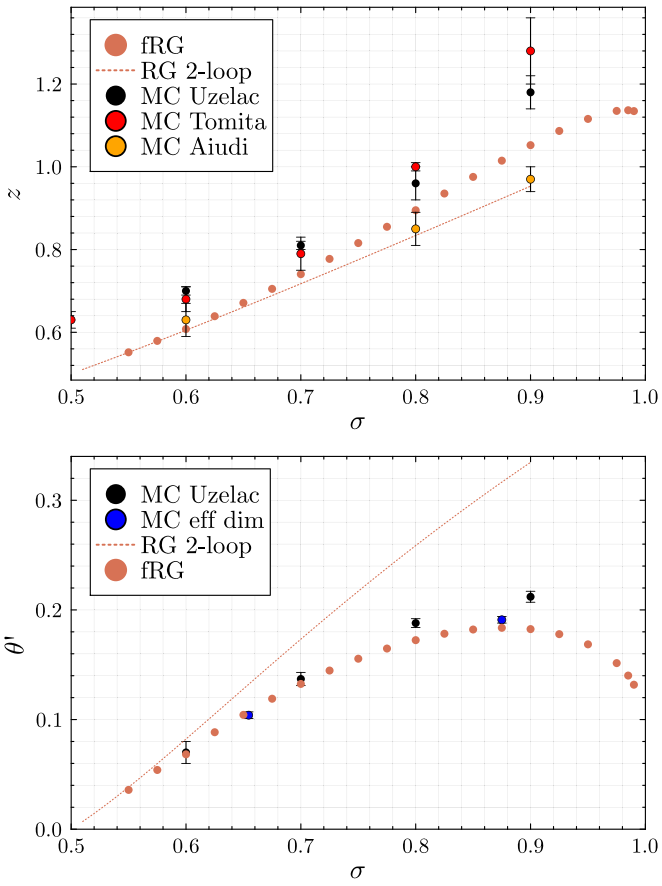


FIG. 1. Dynamical exponents z (upper panel) and θ' (lower panel) for the long-range Ising model in $d = 1$. The dark orange dots are obtained using the fRG scheme described in Sec. IV, with the regulator (45). The dotted lines show the weak-coupling expansions of Ref. [12], which is only valid in the vicinity of $\sigma = 0.5$. The dots with error bars are MC estimates from Ref. [18] (black), Ref. [56] (red), the dynamical Lévy lattice simulations of Ref. [57] (yellow), and, as explained in the main text, Refs. [58–60] via the effective dimension equivalence (blue).

which is a generalization of the Litim regulator [54,55] suitable to the long-range case [22]. This form of the cutoff function allows for an analytic integration of the threshold functions, which are explicitly given in Appendix E. The numerical solution of the differential equation for the effective potential has been obtained using a combination of a shooting approach and a pseudospectral collocation method; the details are found in Ref. [14]. We also remark that, as opposed to the latter study about short-range models, in the long-range case η_K vanishes, thus simplifying the computational procedure.

A. One-dimensional Ising model

We begin with a discussion of results in $d = 1$, due to the existence of MC simulations of the long-range Ising model in one spatial dimension [18,56]. In Fig. 1, we show the dynamical exponent z and the initial-slip exponent θ', defined in Eq. (3), for several values of the range parameter $\sigma \in (\sigma_{\rm mf} = 1/2, \sigma_* = 1)$. For z, we find that our result lies in between the MC points of Refs. [18,56] and the two-loop formula obtained

from the perturbative RG in Ref. [12]. The latter is in good agreement for small σ, which confirms the consistency of our nonperturbative approach in the weak-coupling limit. In addition, Fig. 1 displays MC values obtained through the effective dimension approach of Sec. III, as explained below. We note that, as discussed in more detail in Ref. [14], the accuracy of the present fRG computation can be improved with different regulator choices and extensions of the expansion scheme.

A further, independent benchmark is provided by Ref. [57], where the dynamical exponent is extracted from the critical relaxation time of the long-range Ising chain simulated on a dynamical Lévy lattice, a local algorithm whose validity is established by reproducing the known static exponents. Their estimates are shown in the upper panel of Fig. 1. They lie systematically below the values of Refs. [18,56] and close to the two-loop prediction of Ref. [12], so that for large σ our fRG curve is bracketed from below and from above by independent Monte Carlo results.

In the lower panel of Fig. 1, we plot our results for the initial-slip exponent, which are in good agreement with the MC points of Ref. [18], as well as those coming from the effective dimension approach. Especially for this nonequilibrium critical exponent, a remarkable improvement over the perturbative RG (red dotted curve) is apparent.

We remark that, for both exponents z and θ', the correct behavior as $\sigma \to \sigma_* = 1$ is not known *a priori*. To the best of our knowledge, no previous studies have addressed this regime, and our results therefore constitute the first estimates of the dynamical exponents near the short-range crossover. It is worth noting, however, that even in equilibrium, a similar truncation of the effective action within the fRG framework correctly reproduces the limiting value of the exponent ν as $\sigma \to 1$, but not its approach to this limit (see Ref. [34]). The delicate nature of this region in σ space is related to the fact that the one-dimensional short-range Ising model has no finite-temperature transition. In contrast, in Sec. V C we show that for $d = 2$ our approach correctly captures the crossover to short-range universality as $\sigma \to \sigma_*$.

Finally, let us detail how to apply the effective dimension approach of Sec. III to MC data obtained for short-range Ising models in two and three dimensions. In Ref. [58], we find $(\theta')^{\rm MC}_{\rm SR} = 0.191(3)$ for $D = 2$ and $(\theta')^{\rm MC}_{\rm SR} = 0.104(3)$ for $D = 3$. For the dynamical critical exponents, there exist several MC studies: In $D = 2$, it is found in Ref. [59] that $z^{\rm MC}_{\rm SR} = 2.1667(5)$, while $z^{\rm MC}_{\rm SR} = 2.0245(15)$ in $D = 3$ is reported in Ref. [60]. These results are obtained at a fixed value of the (short-range) dimension D. Using the correspondences (18) and (20), we can compute the LR equivalent of these quantities:

$$z^{\rm MC}_{\rm LR}(\sigma) \equiv \frac{d}{D} z^{\rm MC}_{\rm SR}(D), \tag{46a}$$

$$\theta'^{\rm MC}_{\rm LR}(\sigma) = \theta'^{\rm MC}_{\rm SR}(D), \tag{46b}$$

where $d = 1$, and the two values of σ are obtained from $D = 2$ and $D = 3$ through Eq. (19):

$$\sigma = (2 - \eta_{\rm SR}(D))\frac{d}{D}. \tag{47}$$

Here, $\eta_{\rm SR}(2) = 1/4$, while $\eta_{\rm SR}(3) = \eta_{\rm CB} \approx 0.0363$ is taken from the recent CB work [61]. Therefore, the blue dots of Fig. 1 do not rely on the results of the fRG: This provides an *independent* verification that the effective dimension approach yields estimates of the dynamical exponents that—by visual inspection of the curves in Fig. 1—are in qualitative agreement with the MC results for the long-range Ising chain. However, as discussed in Sec. III, we do not expect that the dimensional correspondence is exact.

B. Long-range critical heat engine

Before a more complete discussion of the dynamical critical O(N) behavior in higher dimensions, here we would like to propose long-range interactions as a possible way to obtain a thermodynamic advantage in the operations of a so-called critical heat engine.

Traditionally, it has been thought that reaching the Carnot efficiency $\eta_{\rm C}$ of a heat engine implies working in the quasistatic limit, i.e., with zero power output $\mathcal{P}$. More generally, there is a trade-off between the power $\mathcal{P}$ and the efficiency η of a thermodynamic heat engine [62]. A way to optimize the ratio $\dot{\Pi} \equiv \mathcal{P}/(\eta_{\rm C} - \eta)$, which we refer to as "performance rate", was proposed in Ref. [25]: One can design a thermodynamic Otto cycle where—instead of a noninteracting substance—the working medium is a system close to its critical point, so that the scaling of the performance rate with the size N of the medium is given by

$$\dot{\Pi} \sim N^{1+\frac{\pi_{\rm th}}{d\nu}}, \tag{48}$$

where $\pi_{\rm th} = \alpha - z\nu$ and α is the specific-heat exponent. Intuitively, the static part comes from the fact that the work output of a single cycle of the engine can be increased by enhancing the specific heat $c \sim |T - T_c|^{-\alpha}$ of the working substance, while operating the engine in finite time requires that the duration of the cycle is at least equal to the relaxation time $\tau_{\rm relax} \sim \xi^z \sim |T - T_c|^{-z\nu}$.

In order to increase the performance rate $\dot{\Pi}$, one aims at the maximization of the exponent $\pi_{\rm th}$. Using long-range systems provides a way of doing so, at least with respect to short-range interacting ones. In fact, a key observation of the present work is that long-range interactions generically facilitate relaxation close to criticality by improving the scaling of $\tau_{\rm relax}$. This may be thought of as a speedup of communication across the system, as a consequence of the enhancement in the cooperation between spins due to their long-range interactions. We quantify this effect via the dynamical exponent z, which already at the mean-field level, $z_{\rm mf} = \sigma$, can be significantly lower than those for the corresponding short-range systems, where we have the rigorous bound $z \geqslant 2$ [63]. The correlations captured by the renormalization group are consistently bringing a positive correction to the value of z, as seen in Figs. 1 and 4. The generality of these observations is corroborated by looking at other systems with long-range interactions, e.g., the long-range Ising model with random impurities, exhibiting an exponent $z = \sigma + O(\sqrt{\epsilon})$ [64], with $\epsilon = 2\sigma - d$, smaller than that of the nearest-neighbor random Ising model (note, however, that introducing quenched disorder tends to have the effect of slowing down relaxation with respect to the pure case).

It is noteworthy that Ref. [25] takes into account the possibility of critical speeding-up, characterized by $z < 0$.

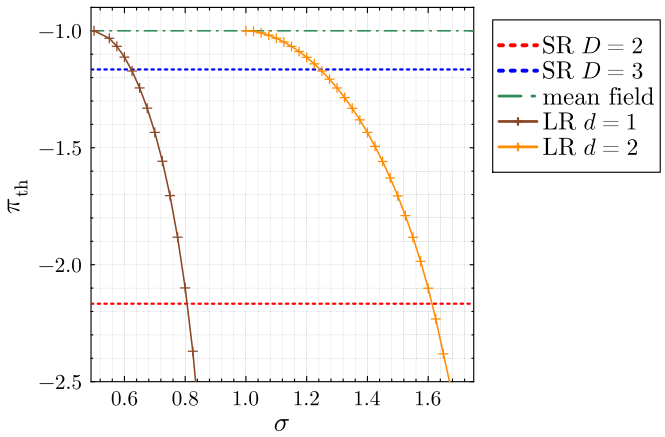


FIG. 2. Performance-rate exponent $\pi_{\rm th} = \alpha - z\nu$ for LR and SR Ising models. The horizontal red and blue dashed lines correspond to the SR Ising model in dimensions $D = 2$ and $D = 3$, respectively. The brown and yellow lines represent the values of the exponent $\pi_{\rm th}$ as σ is varied for the LR Ising model in dimension $d = 1$ and $d = 2$, respectively. The latter curves are obtained by interpolating fRG data points, shown as crosses. The mean-field value $\pi_{\rm th} = -1$, reached by all long-range models at $\sigma_{\rm mf} = d/2$, is visualized as a horizontal green dash-dotted line.

Such behavior is mostly associated either with certain Monte Carlo dynamics [65–67], which, however, do not appear to correspond to physical stochastic evolutions, as classified by Hohenberg and Halperin [8], or with systems exhibiting unconventional relaxation mechanisms (see, e.g., Refs. [68–71]). Nonetheless, it remains plausible that the presence of long-range interactions in such systems could further accelerate thermalization, depending on the specific microscopic pathways to relaxation. Notably, in Ref. [70], where $z < 0$ is experimentally observed at the monopole liquid-gas transition in a spin-ice compound, long-range Coulomb interactions between emergent monopoles are already intrinsic to the system.

On the other hand, the specific-heat exponent α is also generally reduced by the presence of long-range interactions, thus implying that $\pi_{\rm th}$ is not enhanced in both its static and dynamical parts. However, we observe an overall advantage. Using the hyperscaling relation $\alpha = 2 - d\nu$, which holds (within error bars) in the MC simulation [56] of the long-range Ising chain and for self-avoiding Lévy flights [72] in the region $\sigma_{\rm mf} < \sigma < \sigma_*$, enables the usage of the values $\nu(\sigma)$ obtained by some of us for $d = 1$ [34] and $d = 2$ [22]. Hence, we show in Fig. 2 that there are intervals of values of σ where the performance-rate exponent $\pi_{\rm th} = 2 - (d + z)\nu$ is larger than those of the two- and three-dimensional Ising models with short-range interactions. The latter are calculated according to the values reported in Refs. [59–61].

In particular, we notice that $\pi_{\rm th}(\sigma)$ reaches values larger than $\pi_{\rm th}^{\rm SR}(D = 3) \approx -1.17$ as soon as σ is sufficiently close to $\sigma_{\rm mf} = d/2$, where, using the mean-field behavior $z = \nu^{-1} = \sigma$, the dimension-independent result $\pi_{\rm th} = -1$ is obtained. We conclude that long-range interactions with σ close to the mean-field limit yield an enhancement in the scaling of the performance rate $\dot{\Pi}$. This finding aligns with Refs. [73,74], which highlight the thermodynamic advantages of long-range interactions in *quantum* many-body systems. Of course, in the present analysis the possible quantum nature of the system is irrelevant since the heat engine operates at finite temperatures where universal behavior corresponds with the one of the classical theory.

Some remarks are in order: Although the analysis in Ref. [25] mainly addresses the mean work output of the heat engine, the presence of a critical working medium also introduces substantial fluctuations in the work output. These fluctuations pose significant challenges for the practical implementation of macroscopic critical heat engines. However, they can be mitigated in the mesoscopic regime, where finite-size effects regulate critical behavior. In this regime, it becomes possible to design heat engines that simultaneously achieve high power output and large efficiency [75].

More generally, it is desirable to identify working media whose thermodynamic properties exhibit scaling behavior while maintaining a reduced level of fluctuations. In this regard, the phenomenology of short-time universal dynamics—and, in particular, the role of the exponent θ—may prove decisive for future implementations of finite-time critical heat engines. Furthermore, the presence of long-range interactions provides an additional and versatile means to control the system's dynamical evolution. For instance, as discussed in Sec. V C, tuning the crossover time $t_{\rm cross}$ offers a powerful mechanism to foster equilibration in the system.

C. Two-dimensional O(N) models

So far, we have considered the long-range Ising model, corresponding to the case $N = 1$ of the O(N)-symmetric field theory (4). We now extend the analysis to generic O(N) models with $N \geqslant 1$ in $d = 2$, enabling a discussion of the crossover to short-range interactions and a systematic comparison with short-range models through the effective dimension approach of Sec. III.

In Fig. 3, we show the aging exponent $\theta = \theta(\sigma)$ for several values of N. The range of the decay parameter is $\sigma_{\rm mf} = 1 < \sigma < \sigma_*(N)$, where σ_* is the Sak boundary introduced in Sec. II. For $N > 1$, one has $\sigma_*(N) = 2$. In fact, in this case the theory possesses continuous symmetry and the corresponding short-range model in two dimensions cannot have spontaneous symmetry breaking due to the Mermin-Wagner theorem [76], implying $\eta_{\rm SR} = 0$. For $N = 1$, instead, $\sigma_*(1) = 2 - \eta_{\rm SR}$, where $\eta_{\rm SR} = 1/4$ is the anomalous dimension of the two-dimensional Ising model. As is well known [22,24,48], the competition between long- and short-range effects becomes relevant only very close to $\sigma_*(1)$. For this reason, we restrict our analysis to $\sigma \leqslant \sigma_*(1)$; for all $\sigma > \sigma_*(1)$, one recovers the short-range value $\theta(\sigma) \equiv \theta_{\rm SR}$. In the opposite regime $\sigma \to \sigma_{\rm mf} = 1$, all our curves converge to the mean-field result $\theta_{\rm mf} = 0$ anticipated in Sec. II.

We observe a rapid, and uniform in σ, convergence of the aging exponent θ toward its large-N limit (15) as N increases. Defining $\sigma_{\rm int}(N)$ as the intersection point between the finite-N and large-N curves, we find from Fig. 3 that the approach is from below for $\sigma < \sigma_{\rm int}$ and from above otherwise, with $\sigma_{\rm int}$ decreasing as N grows. The case $N = 100$ is indistinguishable from the $N \to \infty$ limit [77]. These benchmarks confirm the robustness of our approach and, in particular, of the truncation (24).

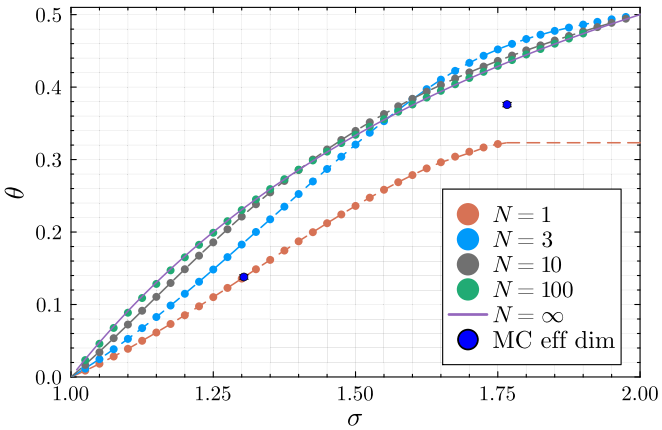


FIG. 3. Aging exponent $\theta = \theta(\sigma)$ for the long-range O(N) models in $d = 2$ with $N = 1, 3, 10, 100$. The colored dots represent data points obtained via the fRG scheme. The large-N limit (15) is denoted by the solid violet line. The dashed lines are $\theta_{\rm SR}(D(\sigma))$ for $N = 1, 3, 10$ obtained from the short-range model through the effective dimension approach of Sec. III. The horizontal dashed line for $N = 1$ starting at $\sigma \approx 1.75$ shows the role of the short-range term in the Ising case for large values of σ. The blue dots are the effective dimension Monte Carlo estimates for $N = 1$, obtained from the short-range model via Eqs. (46a), (47), and (49).

Likewise, we show in Fig. 4 the dynamical exponent z for $d = 2$ and various N. Again, the mean-field limit $z_{\rm mf} = \sigma$ is reached—independent of N—as $\sigma \to \sigma_{\rm mf} = 1$. Similarly, in the short-range limit $\sigma \to \sigma_*$, we retrieve $z = z_{\rm SR}(N = 1) > 2$ for $N = 1$ and $z = 2$ for $N > 1$, in agreement with the Mermin-Wagner theorem. The large-N limit $z = \sigma$ is also approached uniformly from above as N grows larger.

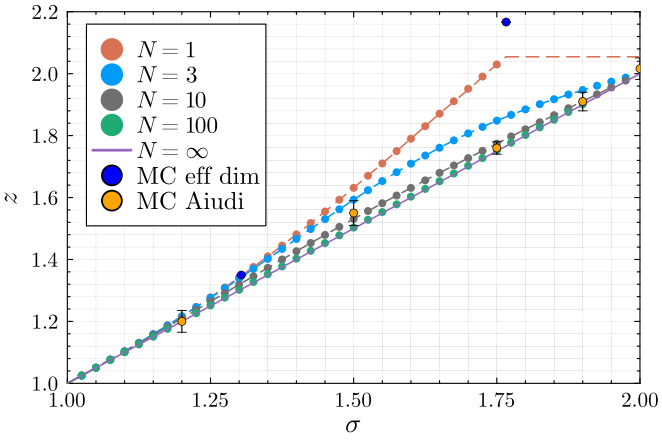


FIG. 4. Dynamical exponent $z = z(\sigma)$ for the long-range O(N) models in $d = 2$ with $N = 1, 3, 10, 100$. The colored dots represent data points obtained via the fRG scheme. The large-N limit $z = \sigma$ is denoted by the solid violet line. The dashed lines are $z_{\rm SR}(D)\, d/D$—cf. Eqs. (18) and (19)—for $N = 1, 3, 10$ obtained from the short-range model through the effective dimension approach. The horizontal dashed line for $N = 1$ has the same meaning as in Fig. 3. The blue dots are effective dimension Monte Carlo estimates for $N = 1$. The yellow dots are the direct long-range MC estimates for $N = 1$ obtained on a dynamical Lévy lattice in Ref. [57].

Moreover, our results, obtained by working directly with the long-range model, match almost perfectly with the short-range ones once the effective dimension approach described in Sec. III is employed. Indeed, we have used the data obtained in Ref. [14] on the critical exponents in fractional dimensions in the range $D \in (2, 4)$ to determine the effective dimension (19) as a continuous function of σ. The dashed curves in Figs. 3 and 4, which overlap almost perfectly with the data points, are not merely guides to the eye: They were obtained independently, that is, via the effective dimension relations (18)–(20) using purely short-range fRG data. In fact, the dimensional equivalence can be observed already at the level of the fRG equations, which can be mapped to their short-range counterparts [14]. This gives further support to our arguments in Sec. III.

The dynamical Lévy lattice simulations of Ref. [57] determine z directly for the two-dimensional long-range Ising model, without recourse to the effective dimension mapping (see Fig. 4). Their estimate is consistent with ours near $\sigma_{\rm mf}$ but a clear discrepancy develops at the Sak boundary: Our flow saturates to the short-range value at $\sigma_*(1) = 2 - \eta_{\rm SR}$, whereas the numerical data follow the free superdiffusive law $z \simeq \sigma$ up to $\sigma = 2$. Reference [57] leaves the location of this dynamical crossover open, noting that settling it requires analytical RG input: Our calculation supplies such input and places it at the static Sak value. We note that simulations of long-range models in this window are known to be affected by strong finite-size corrections [21,30], and that the dynamical Lévy lattice does not satisfy detailed balance, its validation against known critical exponents having been carried out in equilibrium; its dynamical critical behavior therefore lacks an independent benchmark.

Once more, as in Sec. V A, we have incorporated MC results from Refs. [58–60] for the two- and three-dimensional short-range Ising models, mapped to the long-range case via Eqs. (46a), (47), and (49):

$$\theta_{\rm LR}^{\rm MC} = \theta_{\rm SR}^{\rm MC} = \theta'^{\rm MC}_{\rm SR} - \frac{2 - \eta_{\rm SR} - z_{\rm SR}^{\rm MC}}{z_{\rm SR}^{\rm MC}}. \tag{49}$$

As seen in Figs. 3 and 4, these mappings are in reasonable agreement with our fRG values at $\sigma \approx 1.35$ and $\sigma \approx 1.75$, corresponding to $D = 3$ and $D = 2$, respectively. We emphasize again that there is the possibility of an improved calculation of θ and z, especially for larger σ, by choosing more involved truncations and cutoff regulators; see the discussion in Ref. [14].

Compared to the one-dimensional case in Fig. 1, our method shows an even more pronounced improvement over the ϵ expansion of Ref. [12]. Perturbative RG, by its very nature, fails to capture the correct critical behavior near the short-range crossover at $\sigma = \sigma_*$, where $z \to z_{\rm SR}$ and $\theta \to \theta_{\rm SR}$. Moreover, due to the nonmonotonic dependence on N of the function $(N + 2)/(N + 8)^2$ entering the second-order ϵ expansion for z, the perturbative approach predicts spurious degeneracies such as $z(N = 1) = z(N = 10)$ for all σ, which are absent in our nonperturbative treatment.

Finally, starting from the results for the exponents θ and z, we are able to obtain the exponent $\psi = [\theta' + \beta/(\nu z)]^{-1}$ associated with the crossover from short- to long-time universal

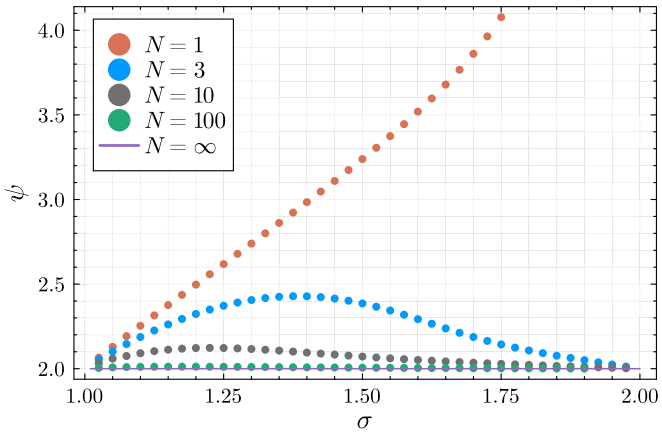


FIG. 5. Exponent ψ vs σ for the long-range models with $N = 1$, 3, 10, 100 in $d = 2$. The colored dots represent values obtained from the same fRG data as Figs. 3 and 4. The large-N limit $\psi = 2$ is plotted as a violet line.

behavior, as discussed in Sec. II. In fact, due to the scaling relation $\beta/\nu = [\phi] = (d - \sigma)/2$,

$$\psi = \left(\theta' + \frac{d-\sigma}{2z}\right)^{-1}, \tag{50}$$

whose large-N limit is $\psi(d, \sigma) \equiv 2$, having used Eq. (15). In Fig. 5, we display the exponent ψ for $d = 2$ and several values of N. If the initial magnetization M_0 is treated as a controllable external parameter, then even small variations in ψ can significantly impact the crossover time $t_{\rm cross} \propto M_0^{-\psi}$. In particular, for very small M_0 one expects a faster crossover to purely relaxational dynamics either when σ is close to its mean-field threshold $\sigma_{\rm mf} = d/2$—where the performance-rate exponent $\pi_{\rm th}$ is also larger, see Fig. 2—or for larger σ in the case $N > 1$.

VI. CONCLUSIONS

In this work, we provided a comprehensive qualitative picture of the dynamics of critical long-range systems using the functional renormalization group, following the methodology of Ref. [14]. Our treatment enabled the derivation of the entire curves of the universal scaling exponents for long-range O(N) models as a function of the symmetry index N, the decay exponent σ, and the dimension d.

For the 1D Ising model (Sec. V A), where MC studies are available, our results closely match numerical predictions. For the dynamical critical exponent z, MC estimates tend to be slightly overestimated, failing to capture leading-order RG behavior near the mean-field limit $\sigma \simeq 0.5$. In contrast, the fRG curve agrees with perturbative results at small σ and deviates toward larger values as $\sigma \to 1$, consistent with the trend set by the MC results. For the aging exponent θ', MC results appear more reliable: They coincide with perturbative estimates at $\sigma \simeq 0.5$ and remain close to the fRG curve for $\sigma < 0.9$. However, the behavior of critical aging as $\sigma \to 1$ remains unclear, though a nonmonotonic trend in scaling indices might be expected from equilibrium studies [34].

In $d = 2$, to our knowledge, there are no numerical studies of critical aging. However, our results can be compared with the scaling indices obtained via the correspondence with the local model [see Eq. (47)], at least for the Ising case. From this perspective, our accuracy remains high up to $\sigma \gtrsim 1.5$, but deviations appear as $\sigma \to \sigma_*$. The magnitude of this deviation is consistent with that expected for LPA′ in local models [14] in $d = 2$. In the present case, however, it is unclear whether this discrepancy stems from the limitations of the LPA′ ansatz or from the approximate nature of the long-range to short-range correspondence [22]. In any case, for higher symmetry groups ($N \geqslant 2$) we expect critical fluctuations to diminish, making the LPA′ ansatz increasingly reliable [78]. This trend is clearly demonstrated by the collapse of our results onto the exactly solvable $N = \infty$ case.

Finally, we note that the applicability of the initial-slip exponent is not confined to quenches at criticality. Recent work [79] shows that the exponent λ governing the long-time decay of the autocorrelation function satisfies $\lambda = d - \theta' z$ also for subcritical quenches ($T < T_c$), thereby extending this relation from critical dynamics to the phase-ordering regime—a result recently confirmed numerically for the 2D Ising universality class in Ref. [80]. This result establishes a direct link between early-time growth, controlled by the initial-slip exponent θ', and long-time aging behavior, pointing to a unified scaling description of critical aging and coarsening. Clarifying how this unified picture is modified by long-range interactions constitutes an interesting direction for future work.

The relevance of studying critical aging at finite temperature lies in its potential thermodynamic applications. Indeed, Ref. [25] shows that employing a working medium near criticality can enhance the performance of an Otto cycle. In this context, we demonstrate that long-range interactions provide an additional knob to achieve a thermodynamic advantage: They generally reduce the dynamical exponent z, thereby shortening cycle times and improving finite-time performance. As a drawback, the specific-heat exponent α decreases under long-range interactions, yet the combined effect still leads to an overall enhancement of the performance-rate exponent $\pi_{\rm th}$ near the mean-field limit (see Fig. 2). Our findings thus highlight how tuning universal behavior through long-range interactions offers a robust pathway to thermodynamic advantage.

Further thermodynamic applications of long-range many-body systems may arise in quantum thermodynamics [74], where questions on universal dynamical scaling and critical aging intertwine with fundamental issues of prethermalization and equilibration [81]. Addressing these challenges may require extending the LPA′ ansatz (cf. Ref. [82] at equilibrium) to capture the chaotic nature of dynamics beyond one loop [83]. In this context, it could also be possible to incorporate the effects of (long-range) correlated disorder, whose impact on universality closely resembles that of long-range interactions [84].

ACKNOWLEDGMENTS

N.D. is grateful to M. Campisi for useful discussions that inspired this work. V.P. acknowledges G. Piccitto for her useful comments on the role of fluctuations in critical heat engines. This research was funded by the Swiss National Science Foundation (SNSF) Grants No. 200021–207537 and

No. 200021–236722, by the Deutsche Forschungsgemeinschaft (DFG, German Research Foundation) under Germany's Excellence Strategy EXC2181/1-390900948 (the Heidelberg STRUCTURES Excellence Cluster), and the Swiss State Secretariat for Education, Research and Innovation (SERI). Partial support by grant NSF Grant No. PHY-2309135 to the Kavli Institute for Theoretical Physics (KITP) is also acknowledged.

DATA AVAILABILITY

The data that support the findings of this article are not publicly available. The data are available from the authors upon reasonable request.

APPENDIX A: DYNAMICAL SCALING IN THE LARGE-N LIMIT

In this Appendix, we summarize how the decoupling (11) allows us to obtain an analytic expression for the scaling form of correlation functions and, as a consequence, for the dynamical exponents z and θ. First, the Gaussian correlators are provided. After that, we outline the self-consistent procedure based on Eq. (13).

1. Response and correlation functions

In the quadratic theory describing the large-N limit, it is found (cf. Ref. [10]) that, as a generalization of Eq. (9b),

$$G^R(\boldsymbol{q},t,t') = \vartheta(t-t')e^{-\int_{t'}^{t}[q^\sigma+\tau_C(u)]\,du}, \tag{A1}$$

where $\tau_0^{-1}=0$ has been set. The bare dispersion relation $q^\sigma+\tau$ has been replaced by $q^\sigma+\tau_C(t)$. On the other hand,

$$G^C(\boldsymbol{q},t,t') = 2\int_{t_0}^{\infty} G^R(\boldsymbol{q},t,u)G^R(\boldsymbol{q},t',u)\,du. \tag{A2}$$

In the infinite-time limit $C(\boldsymbol{q},\infty)=(q^\sigma+\tau_C(\infty))^{-1}$, with $\tau_C(\infty)=\xi^{-2}$, is the Gaussian correlation function in equilibrium.

2. Self-consistent calculation

Let us start with the equal-time correlator, whose scaling behavior at criticality ($\tau_C\to 0$) is taken to be the same as that of Eq. (9a) for $t'=t$, i.e.,

$$C(\boldsymbol{q},t) = \frac{1}{q^\sigma}F(2q^\sigma t), \quad F(s)=\begin{cases}0, & \text{if } s=0,\\ 1, & \text{if } s=\infty.\end{cases} \tag{A3}$$

On the other hand, since τ and q^σ have the same dimensions, we are allowed to make the ansatz

$$\tau_C(t) = \frac{\gamma}{2t}, \tag{A4}$$

provided that γ is a dimensionless constant, and, in particular, time independent. Now, the crucial point is that the time-dependent coupling and the equal-time correlator have to obey the self-consistency equation (13), which can be rewritten as

$$\tau_C(t) = \tau_C(\infty) + \frac{g}{6}\int_{\boldsymbol{q}}[C(\boldsymbol{q},t)-C(\boldsymbol{q},\infty)]. \tag{A5}$$

As shown below, this implies that the only consistent solution for γ is $\gamma=d/\sigma-2$. Furthermore, we are going to find that the aging exponent θ is related to γ.

In fact, inserting Eq. (A4) into Eq. (A2) yields a result compatible with Eq. (A3), and, in particular, allows to determine the scaling function:

$$F(s) = s\int_0^1 dy\,(1-y)^\gamma e^{-sy} \quad (\gamma>-1). \tag{A6}$$

We are now ready to evaluate Eq. (A5) at criticality ($\tau_C(\infty)=0$), which gives the following condition for γ:

$$\begin{aligned}\gamma &= 2t\,\frac{g_*}{6}\frac{\Omega_d}{(2\pi)^d}\int_0^\Lambda dq\,q^{d-1-\sigma}[F(2q^\sigma t)-1]\\ &= \frac{g_*}{6\sigma}\frac{\Omega_d}{(2\pi)^d}(2t)^{\frac{\epsilon}{\sigma}}\int_0^{2t\Lambda^\sigma} ds\,s^{-\frac{\epsilon}{\sigma}}[F(s)-1],\end{aligned} \tag{A7}$$

where Λ is an ultraviolet cutoff for momentum integrals, $\Omega_d=2\pi^{d/2}/\Gamma(d/2)$, $\epsilon=2\sigma-d>0$, and g_* is the fixed-point value of the quartic coupling g. Next, we split the integral into two parts:

$$\int_0^\infty ds\,s^{-\frac{\epsilon}{\sigma}}[F(s)-1] - \int_{2t\Lambda^\sigma}^\infty ds\,s^{-\frac{\epsilon}{\sigma}}[F(s)-1]. \tag{A8}$$

The first integral must be zero, because otherwise its prefactor in Eq. (A7) would give a t-dependent contribution $\propto t^{\epsilon/\sigma}$ to γ, which is ruled out by γ being dimensionless:

$$0 = \int_0^\infty ds\,s^{-\frac{\epsilon}{\sigma}}[F(s)-1] \propto \Gamma(\gamma+\epsilon/\sigma)^{-1}, \tag{A9}$$

having integrated by parts and noticed that the boundary terms vanish. Thus, we have to pick one of the poles of the Gamma function. The only solution allowed by the condition $\gamma>-1$ in Eq. (A6) is

$$\gamma = -\epsilon/\sigma = d/\sigma - 2. \tag{A10}$$

Evaluating the second integral in the regime $t\gg(2\Lambda^\sigma)^{-1}$ (discarding nonuniversal details at microscopically short times) would also enable the determination of g_* [10].

Using Eqs. (A4) and (A10), the critical form of the response function [Eq. (A1)] is then

$$G^R(\boldsymbol{q},t,t') = \vartheta(t-t')(t/t')^\theta e^{-q^\sigma(t-t')}, \tag{A11}$$

with $\theta=-\gamma/2=1-d/(2\sigma)$.

APPENDIX B: FUNCTIONAL DERIVATIVES IN SYSTEMS WITH BOUNDARIES

Let us consider a system on the manifold $\mathcal{M}$, whose boundary is $\mathcal{B}=\partial\mathcal{M}$. In our case, the manifold is flat: $\mathcal{M}\subset\mathbb{R}^D$, for some integer D. Given a functional

$$J[\phi] = \int_{\mathcal{M}} dV\, f(\phi,\nabla\phi) + \int_{\mathcal{B}} dA\, g(\phi), \tag{B1}$$

upon the variation of the function from ϕ to $\phi+\delta\phi$,

$$\begin{aligned}\delta_\phi J = &\int_{\mathcal{M}} dV\left[\frac{\partial f}{\partial\phi} - \boldsymbol{\nabla}\cdot\left(\frac{\partial f}{\partial(\nabla\phi)}\right)\right]\delta\phi\\ &+\int_{\mathcal{B}} dA\left[\frac{\partial f}{\partial(\boldsymbol{\nabla}\phi)}\cdot\boldsymbol{n}+\frac{\partial g}{\partial\phi}\right]_{\phi=\phi_{\mathcal{B}}}\delta\phi_{\mathcal{B}},\end{aligned} \tag{B2}$$

where the function on the boundary is denoted by $\phi_{\mathcal{B}}$ and $\boldsymbol{n}$ is the unit vector normal to the boundary. As hinted by the notation, we identify ϕ with the order-parameter field $\phi(t,\boldsymbol{x})$, and for simplicity we neglect its spatial dependence. Then, the manifold $\mathcal{M}$ is $[t_0,\infty) \ni t$, the temporal "bulk", while the boundary is just $\mathcal{B} = \{t_0\}$. Denoting $\partial_t\phi \equiv \dot{\phi}$, one has $f = f(\phi,\dot{\phi})$ and

$$\delta_\phi J = \int_{t_0}^{\infty} dt \left[\frac{\partial f}{\partial \phi} - \partial_t\left(\frac{\partial f}{\partial \dot{\phi}}\right)\right]\delta\phi + \left[-\frac{\partial f}{\partial \dot{\phi}} + \frac{\partial g}{\partial \phi}\right]_{\phi=\phi_0}\delta\phi_0. \tag{B3}$$

1. Variations of the effective average action

Clearly, we want to compute the variations of ansatz (24). Hereafter, let us write $\int_t \equiv \int_{t_0}^{\infty}$ as a shorthand notation for time integrals. Then,

$$\Gamma[\boldsymbol{\phi},\tilde{\boldsymbol{\phi}}] = \int_t \tilde{\phi}_i(t)[Z\dot{\phi}_i(t) + Kq^\sigma\phi_i(t) - \Omega\tilde{\phi}_i(t) + V^{(i)}(\boldsymbol{\phi}(t))] + \left(Z_0\tilde{\phi}_{0,i}\phi_{0,i} - \frac{Z_0^2}{2\tau_0}\tilde{\phi}_{0,i}^2\right), \tag{B4}$$

meaning that

$$f(\Phi,\dot{\Phi}) = \tilde{\phi}_i[Z\dot{\phi}_i + Kq^\sigma\phi_i - \Omega\tilde{\phi}_i + V^{(i)}(\boldsymbol{\phi})], \tag{B5}$$

$$g(\Phi) = Z_0\tilde{\phi}_i\phi_i - \frac{Z_0^2}{2\tau_0}\tilde{\phi}_i^2, \tag{B6}$$

where concretely one can read $\Phi = \phi_j$ or $\Phi = \tilde{\phi}_j$ according to which field we are choosing when performing the variation. Using Eq. (B3), one obtains the following results:

$$\delta_{\phi_i}\Gamma = \int_t [\tilde{\phi}_i Kq^\sigma + \tilde{\phi}_j V^{(ij)}(\boldsymbol{\phi}) - Z\dot{\tilde{\phi}}_i]\delta\phi_i + (Z_0 - Z)\tilde{\phi}_{0,i}\delta\phi_{0,i}, \tag{B7a}$$

$$\delta_{\tilde{\phi}_i}\Gamma = \int_t \{[Z\dot{\phi}_i + Kq^\sigma\phi_i + V^{(i)}(\boldsymbol{\phi})] - 2\Omega\tilde{\phi}_i\}\delta\tilde{\phi}_i + \left(Z_0\phi_{0,i} - \frac{Z_0^2}{\tau_0}\tilde{\phi}_{0,i}\right)\delta\tilde{\phi}_{0,i}, \tag{B7b}$$

and

$$\delta^2_{\tilde{\phi}_i\tilde{\phi}_j}\Gamma = \delta_{ij}\int_t(-2\Omega)\delta\tilde{\phi}_i\delta\tilde{\phi}_j - \delta_{ij}\frac{Z_0^2}{\tau_0}\delta\tilde{\phi}_{0,i}\delta\tilde{\phi}_{0,j}, \tag{B8a}$$

$$\delta^2_{\phi_i\tilde{\phi}_j}\Gamma = \int_t \{[Kq^\sigma\delta_{ij} + V^{(ij)}(\boldsymbol{\phi})]\delta\phi_i + \delta_{ij}Z\partial_t\delta\phi_i\}\delta\tilde{\phi}_j + \delta_{ij}Z_0\delta\phi_{0,i}\delta\tilde{\phi}_{0,j}, \tag{B8b}$$

$$\delta^2_{\tilde{\phi}_i\phi_j}\Gamma = \int_t \{[Kq^\sigma\delta_{ij} + V^{(ij)}(\boldsymbol{\phi})]\delta\tilde{\phi}_i - \delta_{ij}Z\partial_t\delta\tilde{\phi}_i\}\delta\phi_j + \delta_{ij}(Z_0 - Z)\delta\tilde{\phi}_{0,i}\delta\phi_{0,j}. \tag{B8c}$$

The relations (B8), together with the obvious $\delta^2_{\phi_i\phi_j}\Gamma$ involving only derivatives of the effective potential, form the Hessian matrix $\Gamma^{(2)}$.

2. Variations of the Wetterich equation

Let us now consider the right-hand side of Eq. (21),

$$\frac{\partial_\kappa R}{2}\int_t \mathrm{tr}[\mathbb{G}(t,t)\hat{\tau}_1] \equiv \frac{\partial_\kappa R}{2}\mathcal{J}[\boldsymbol{\phi},\tilde{\boldsymbol{\phi}}], \tag{B9}$$

where the trace is over the 2×2 matrix structure of the response field framework [and possibly over $\mathrm{O}(N)$ indices if $N > 1$]. Ignoring the prefactor, we make the identifications $f(\Phi) = \mathrm{tr}[\mathbb{G}(t,t)\hat{\tau}_1]$ (where f is independent of derivatives of the field, as the propagator is so) and $g(\Phi) = 0$. Calculating the first and second variations of the Wetterich equation with respect to ϕ and $\tilde{\phi}$ allows us to compare with the results of Appendix B 1 and obtain the flow of the potential (43) and the other renormalization functions. One immediately sees that

$$\delta^2_{\phi_i\tilde{\phi}_j}\mathcal{J}[\boldsymbol{\phi},\tilde{\boldsymbol{\phi}}] = \int_t \mathrm{tr}\left\{\delta^2_{\phi_i\tilde{\phi}_j}\mathbb{G}(t,t)\hat{\tau}_1\right\}, \tag{B10}$$

and similarly for the other variations, where, due to Eq. (22),

$$\delta_\Phi\mathbb{G}(t_1,t_2) = -[\mathbb{G}(\delta_\Phi\Gamma^{(2)})\mathbb{G}](t_1,t_2) = -\int_{t'}\mathbb{G}(t_1,t')(\delta_\Phi\Gamma^{(2)})\mathbb{G}(t',t_2), \tag{B11}$$

since the genuine time dependence is contained in the propagator matrix, as motivated below. To compare the right- and left-hand sides of Eq. (21), one needs to rewrite $\delta_\Phi\Gamma^{(2)} = \int_t \frac{\delta\Gamma^{(2)}}{\delta\Phi}\delta\Phi$, where $\frac{\delta\Gamma^{(2)}}{\delta\Phi}$ is the functional derivative, and notice that the variation $\delta\Phi$ is arbitrary.

APPENDIX C: INVERSION OF THE HESSIAN

As discussed in Sec. IV C, on the stationary background $\boldsymbol{\Phi}_u$ the regulated Hessian decomposes into one longitudinal and $N-1$ identical transverse sectors, with renormalized dispersions given in Eq. (32). Here, we provide its explicit inversion, first in the time-translation-invariant limit and then in the presence of the initial-time boundary.

In the limit $t_0 \to -\infty$, time-translation invariance is restored and the Hessian can be transformed to frequency space. Its 2×2 block in correlation-response field space, for each sector $i \in \{L,T\}$, is

$$\left(\mathbb{G}_k^{-1}\right)_i = \begin{pmatrix} 0 & P_k^i(\omega,q^\sigma) \\ P_k^i(-\omega,q^\sigma) & -2\Omega_k \end{pmatrix}, \tag{C1}$$

where $P_k^i(\omega,q^\sigma) \equiv Z_k i\omega + \omega_{i,k}(q^\sigma)$. Now, the inversion can be performed independently in the longitudinal and transverse sectors, yielding

$$\mathbb{G}_{k,i}(\omega,\boldsymbol{q}) = \begin{pmatrix} \frac{2\Omega_k}{P_k^i(\omega,q^\sigma)P_k^i(-\omega,q^\sigma)} & \frac{1}{P_k^i(-\omega,q^\sigma)} \\ \frac{1}{P_k^i(\omega,q^\sigma)} & 0 \end{pmatrix}. \tag{C2}$$

An inverse Fourier transform gives the time-translation-invariant correlation and response functions reported in Eqs. (33) and (34).

At finite t_0, time-translation invariance is broken and the Hessian cannot be inverted by a Fourier transform in time. To retain the boundary contribution, we decompose the inverse propagator into a field-independent and a field-dependent part,

$$\mathbb{G}^{-1}(x,x';\boldsymbol{\Phi}) = \mathbb{G}_0^{-1}(x,x') + \mathbb{V}(x,x';\boldsymbol{\Phi}), \tag{C3}$$

where $\mathbb{V}(x,x';\mathbf{\Phi}) = \delta(x-x')\vartheta(t-t_0)\mathbb{V}(x;\mathbf{\Phi})$ and using the notation $x=(t,\boldsymbol{x})$. The field-dependent contribution reads

$$\mathbb{V}_{ij}(x;\mathbf{\Phi}) = \begin{pmatrix} \tilde{\phi}_l V_k^{(ijl)}(\boldsymbol{\phi}) & \delta_{ij}\big[V_k^{(ii)}(\boldsymbol{\phi}) - V_k^{(ii)}(\boldsymbol{\phi}_u)\big] \\ \delta_{ij}\big[V_k^{(ii)}(\boldsymbol{\phi}) - V_k^{(ii)}(\boldsymbol{\phi}_u)\big] & 0 \end{pmatrix}, \tag{C4}$$

while the field-independent part is obtained from the quadratic terms of Γ_k (see below). On the stationary background $\mathbf{\Phi}_u = (\boldsymbol{\phi}_u, \mathbf{0})$, the field-dependent contribution $\mathbb{V}$ vanishes, so that $\mathbb{G}^{-1} = \mathbb{G}_0^{-1}$. We stress that the splitting in Eq. (C3) is valid also for $t_0 \to -\infty$: $\mathbb{V}$ vanishes on the stationary background in both temporal regimes.

Then, the only task left is to obtain the explicit form of $\mathbb{G}_0$. It proves convenient to treat the boundary and bulk fields as separate components of enlarged field vectors. For each sector $i \in \{L,T\}$ and momentum $\boldsymbol{q}$, we define

$$\Phi \equiv \begin{pmatrix} \phi_0 \\ \phi(t) \end{pmatrix}, \quad \widetilde{\Phi} \equiv \begin{pmatrix} \tilde{\phi}_0 \\ \tilde{\phi}(t) \end{pmatrix}, \quad t > t_0, \tag{C5}$$

with the matching condition $\phi(t_0^+) = \phi_0$. The sector index on the fields is suppressed in the following. For two generic boundary-bulk vectors of the form $X = (X_0\ X(t))^T$, we define an inner product

$$\langle X, X'\rangle \equiv X_0 X_0' + \int_{t_0}^{\infty} dt\, X(t)X'(t). \tag{C6}$$

We introduce the operators $\mathcal{L}_{i,k}$ and $\mathcal{Q}_k$ through their actions on Φ and $\tilde{\Phi}$, respectively:

$$\mathcal{L}_{i,k}\Phi \equiv \begin{pmatrix} Z_{0,k}\phi_0 \\ [Z_k\partial_t + \omega_{i,k}(q^\sigma)]\phi(t) \end{pmatrix}, \quad \mathcal{Q}_k\widetilde{\Phi} \equiv \begin{pmatrix} \frac{Z_{0,k}^2}{2\tau_0}\tilde{\phi}_0 \\ \Omega_k\tilde{\phi}(t) \end{pmatrix}. \tag{C7}$$

The quadratic effective action on the stationary background can then be written as

$$\begin{aligned}\Gamma_{0,k}^{(i)} &= \langle\widetilde{\Phi}, \mathcal{L}_{i,k}\Phi\rangle - \langle\widetilde{\Phi}, \mathcal{Q}_k\widetilde{\Phi}\rangle \\ &= Z_{0,k}\tilde{\phi}_0\phi_0 - \frac{Z_{0,k}^2}{2\tau_0}\tilde{\phi}_0^2 + \int_{t_0}^{\infty} dt \\ &\quad\times\{\tilde{\phi}(t)[Z_k\partial_t + \omega_{i,k}(q^\sigma)]\phi(t) - \Omega_k\tilde{\phi}(t)^2\}.\end{aligned} \tag{C8}$$

The adjoint $\mathcal{L}_{i,k}^\dagger$, defined by $\langle\widetilde{\Phi}, \mathcal{L}_{i,k}\Phi\rangle = \langle\mathcal{L}_{i,k}^\dagger\widetilde{\Phi}, \Phi\rangle$, acts on the response-field vector as

$$\mathcal{L}_{i,k}^\dagger\widetilde{\Phi} = \begin{pmatrix} Z_{0,k}\tilde{\phi}_0 - Z_k\tilde{\phi}(t_0^+) \\ [-Z_k\partial_t + \omega_{i,k}(q^\sigma)]\tilde{\phi}(t) \end{pmatrix}, \tag{C9}$$

as it is verified by integrating the time-derivative term by parts.

We now further collect the order-parameter and response-field vectors into $\Psi \equiv (\Phi\ \widetilde{\Phi})^T$ and extend the inner product according to $\langle\Psi,\Psi'\rangle \equiv \langle\Phi,\Phi'\rangle + \langle\widetilde{\Phi},\widetilde{\Phi}'\rangle$. The quadratic action thus becomes

$$\Gamma_{0,k}^{(i)} = \frac{1}{2}\langle\Psi, \mathcal{A}_{i,k}\Psi\rangle, \quad \mathcal{A}_{i,k} \equiv \mathcal{G}_{0,i}^{-1} = \begin{pmatrix} 0 & \mathcal{L}_{i,k}^\dagger \\ \mathcal{L}_{i,k} & -2\mathcal{Q}_k \end{pmatrix}. \tag{C10}$$

The inverse of this block operator is

$$\mathcal{G}_{0,i} \equiv \begin{pmatrix} \mathcal{G}_{0,i}^C & \mathcal{G}_{0,i}^R \\ \mathcal{G}_{0,i}^A & 0 \end{pmatrix} = \mathcal{A}_{i,k}^{-1} = \begin{pmatrix} 2\mathcal{L}_{i,k}^{-1}\mathcal{Q}_k\mathcal{L}_{i,k}^{-\dagger} & \mathcal{L}_{i,k}^{-1} \\ \mathcal{L}_{i,k}^{-\dagger} & 0 \end{pmatrix},$$
$$\text{with}\ \ \mathcal{L}_{i,k}^{-\dagger} \equiv (\mathcal{L}_{i,k}^\dagger)^{-1} = \big(\mathcal{L}_{i,k}^{-1}\big)^\dagger. \tag{C11}$$

The enlarged propagator $\mathcal{G}_{0,i}$ contains all boundary-boundary, boundary-bulk, and bulk-bulk correlation and response functions. The propagator $\mathbb{G}_{0,i}(t,t')$ used in the flow equations is its restriction to the bulk sector:

$$\mathbb{G}_{0,ij}(t,t') = \delta_{ij}\begin{pmatrix} G_{0,i}^C(t,t') & G_{0,i}^R(t,t') \\ G_{0,i}^R(t',t) & 0 \end{pmatrix}, \quad t,t' > t_0. \tag{C12}$$

To determine $\mathcal{L}_{i,k}^{-1}$, we solve the linear problem $\mathcal{L}_{i,k}\Phi = J$, with $J = (j_0\ j(t))^T$. In components, this gives

$$Z_{0,k}\phi_0 = j_0, \tag{C13a}$$
$$[Z_k\partial_t + \omega_{i,k}(q^\sigma)]\phi(t) = j(t), \quad t > t_0, \tag{C13b}$$

together with the matching condition $\phi(t_0^+) = \phi_0$. Its solution is $\phi_0 = j_0/Z_{0,k}$ and

$$\phi(t) = \frac{j_0}{Z_{0,k}}e^{-\omega_{i,k}(q^\sigma)(t-t_0)/Z_k} + \frac{1}{Z_k}\int_{t_0}^{\infty} dt'\,\vartheta(t-t')e^{-\omega_{i,k}(q^\sigma)(t-t')/Z_k}j(t'). \tag{C14}$$

Therefore,

$$\mathcal{L}_{i,k}^{-1} = \begin{pmatrix} \frac{1}{Z_{0,k}} & 0 \\ \frac{e^{-\omega_{i,k}(q^\sigma)(t-t_0)/Z_k}}{Z_{0,k}} & \frac{\vartheta(t-t')e^{-\omega_{i,k}(q^\sigma)(t-t')/Z_k}}{Z_k} \end{pmatrix},$$
$$\mathcal{L}_{i,k}^{-\dagger} = \begin{pmatrix} \frac{1}{Z_{0,k}} & \frac{e^{-\omega_{i,k}(q^\sigma)(t'-t_0)/Z_k}}{Z_{0,k}} \\ 0 & \frac{\vartheta(t'-t)e^{-\omega_{i,k}(q^\sigma)(t'-t)/Z_k}}{Z_k} \end{pmatrix}. \tag{C15}$$

The bulk-bulk terms of Eq. (C15) immediately give, through Eq. (C11),

$$G_{0,i}^R(t,t') = \frac{\vartheta(t-t')}{Z_k}e^{-\omega_{i,k}(q^\sigma)(t-t')/Z_k},$$
$$G_{0,i}^A(t,t') = \frac{\vartheta(t'-t)}{Z_k}e^{-\omega_{i,k}(q^\sigma)(t'-t)/Z_k} = G_{0,i}^R(t',t). \tag{C16}$$

Finally, a short calculation reveals that the bulk-bulk component of $\mathcal{G}_{0,i}^C = 2\mathcal{L}_{i,k}^{-1}\mathcal{Q}_k\mathcal{L}_{i,k}^{-\dagger}$ is given by

$$G_{0,i}^C(t,t') = \frac{1}{\tau_0}e^{-\omega_{i,k}(q^\sigma)(t+t'-2t_0)/Z_k} + \frac{2\Omega_k}{Z_k^2}\int_{t_0}^{\min(t,t')} ds\, e^{-\omega_{i,k}(q^\sigma)(t+t'-2s)/Z_k} \tag{C17}$$

$$= \frac{\Omega_k}{Z_k \omega_{i,k}(q^\sigma)} e^{-\omega_{i,k}(q^\sigma)|t-t'|/Z_k} + \left[\frac{1}{\tau_0} - \frac{\Omega_k}{Z_k \omega_{i,k}(q^\sigma)}\right] e^{-\omega_{i,k}(q^\sigma)(t+t'-2t_0)/Z_k}. \tag{C18}$$

Compared to the equilibrium correlation and response functions [Eq. (34)], only the correlator receives a correction that breaks time-translation invariance, while $G^R_{0,i}(t,t') = G^R_{\mathrm{eq},i}(t,t')$. This correction,

$$G^C_{\mathrm{neq},i}(t,t') = \frac{\gamma_{i,k}}{\omega_{i,k}(q^\sigma)} e^{-\omega_{i,k}(q^\sigma)(t+t'-2t_0)/Z_k}, \qquad \gamma_{i,k} \equiv \frac{\omega_{i,k}(q^\sigma)}{\tau_0} - \frac{\Omega_k}{Z_k}, \tag{C19}$$

vanishes in the limit $t_0 \to -\infty$ or $t + t' \to \infty$. Moreover, independent of the values of $Z_k, \Omega_k, Z_{0,k}$, one finds $G^C_{0,i}(t_0,t_0) = \frac{1}{\tau_0}$, as required by the prescribed initial distribution [Eq. (8)].

APPENDIX D: CALCULATION OF THE FLOW EQUATIONS

Throughout this Appendix, we work directly in the case $\tau_0 = \infty$ (cf. Sec. II). Thus, the coefficient $\gamma_{i,k}$ in the nonequilibrium part of Eq. (C18) becomes independent of the N-component: $\gamma_{i,k} = \gamma_k$. We illustrate here only the calculation of the flows of $Z_{0,k}$ and Ω_k, but those of the other quantities are obtained in a very similar manner.

1. Flow of Z_0

Let us consider the RG-time derivatives of (B8b) and (B10) on the temporal boundary. Comparing them yields

$$\delta_{ij}\partial_\kappa Z_0\, \delta\phi_{0,i}\delta\tilde{\phi}_{0,j} = \frac{\partial_\kappa R}{2}\int_t \mathrm{tr}\left\{\delta^2_{\phi_i\tilde{\phi}_j}\mathbb{G}(t,t)\hat{\tau}_1\right\} \equiv \frac{\partial_\kappa R}{2}\mathcal{I}_{ij}. \tag{D1}$$

We immediately see that in order to find $\delta\phi_{0,i}$ and $\delta\tilde{\phi}_{0,i}$ on the right-hand side of the previous equation we need to use the procedure described in Appendix F. Let us split the integral as $\mathcal{I}_{ij} = \mathcal{I}^{\mathrm{a}}_{ij} + \mathcal{I}^{\mathrm{b}}_{ij}$, with

$$\mathcal{I}^{\mathrm{a}}_{ij} = \sum_{a,b=1}^{N}\int_{t,t',t''} \mathrm{tr}\Big\{\Big[\mathbb{G}_a(t,t'')\big(\delta_{\tilde{\phi}_j}\Gamma^{(2)}\big)_{ab}\mathbb{G}_b(t'',t')\big(\delta_{\phi_i}\Gamma^{(2)}\big)_{ba}\mathbb{G}_a(t',t) + \mathbb{G}_a(t,t')\big(\delta_{\phi_i}\Gamma^{(2)}\big)_{ab}\mathbb{G}_b(t',t'')\big(\delta_{\tilde{\phi}_j}\Gamma^{(2)}\big)_{ba}\mathbb{G}_a(t'',t)\Big]\hat{\tau}_1\Big\}, \tag{D2a}$$

$$\mathcal{I}^{\mathrm{b}}_{ij} = -\sum_{a=1}^{N}\int_{t,t'} \mathrm{tr}\left\{\mathbb{G}_a(t,t')\big(\delta^2_{\phi_i\tilde{\phi}_j}\Gamma^{(2)}\big)_{aa}\mathbb{G}_a(t',t)\hat{\tau}_1\right\}. \tag{D2b}$$

For practical convenience, we compute the integrals over t and t'' first, while leaving the t' integral for later. We find that the time dependence enters only through the combination $(t' - t_0)$. In particular,

$$\mathcal{I}^{\mathrm{b}}_{ii} = \sum_{a=1}^{N}\frac{V^{(aaii)}(\boldsymbol{\phi})}{\omega_a^2 Z_k}\int_{t'}(e^{-2\omega_a(t'-t_0)/Z_k}[\Omega_k - 2\gamma\omega_a(t'-t_0)] - \Omega_k)\delta\phi_i\delta\tilde{\phi}_i, \tag{D3}$$

and a much longer expression for $\mathcal{I}^{\mathrm{a}}_{ii}$, which we do not display here, but it is again an integral over t' where the time-dependent part of the integrand is proportional to $e^{-3(\omega_a+\omega_b)(t'-t_0)/Z}$. We can now employ the short-time trick described in Appendix F to obtain the variation at the time-boundary $t' = t_0$ and compare the result with the left-hand side. Using Eq. (F4), we obtain

$$\mathcal{I}^{\mathrm{b}}_{ii}(t_0) = \sum_{a=1}^{N}\frac{V^{(aaii)}(\boldsymbol{\phi})}{2\omega_a^3}(\Omega_k - Z_k\gamma)\delta\phi_{0,i}\delta\tilde{\phi}_{0,i}, \tag{D4a}$$

$$\mathcal{I}^{\mathrm{a}}_{ii}(t_0) = -\sum_{a,b=1}^{N}V^{(abi)}(\boldsymbol{\phi})^2\frac{\omega_b^2\Omega_k(\omega_a+\omega_b) - Z_k\gamma\left(2\omega_a\omega_b^2 + \omega_a^3 + \omega_b^3\right)}{\omega_a^3\omega_b^2(\omega_a+\omega_b)^2}\delta\phi_{0,i}\delta\tilde{\phi}_{0,i}, \tag{D4b}$$

once we evaluate on a constant field configuration (in particular, with $\tilde{\boldsymbol{\phi}} = 0$). Finally, if $i = m = 1$,

$$\partial_\kappa Z_0 = \int_{\boldsymbol{q}}\frac{\partial_\kappa R}{2}\left[-V_k^{(111)}(\boldsymbol{\phi})^2\frac{\Omega_k - 2Z_k\gamma}{2\omega_L^4} - (N-1)V_k^{(1gg)}(\boldsymbol{\phi})^2\frac{\Omega_k - 2Z_k\gamma}{2\omega_T^4} + \frac{\Omega_k - Z_k\gamma}{2}\left\{\frac{V_k^{(1111)}(\boldsymbol{\phi})}{\omega_L^3} + (N-1)\frac{V_k^{(11gg)}(\boldsymbol{\phi})}{\omega_T^3}\right\}\right], \tag{D5}$$

or if $i = g \neq 1$,

$$\partial_\kappa Z_0 = \int_{\boldsymbol{q}} \frac{\partial_\kappa R}{2}\Bigg[-V_k^{(1gg)}(\boldsymbol{\phi})^2 \frac{\Omega_k\left(\omega_L^4+\omega_L^3\omega_T+\omega_L\omega_T^3+\omega_T^4\right)-\gamma Z_k\left(\omega_L^4+3\omega_L^3\omega_T+3\omega_L\omega_T^3+\omega_T^4\right)}{(\omega_L+\omega_T)^2\omega_L^3\omega_T^3} + \frac{\Omega_k - Z_k\gamma}{2}\left\{\frac{V_k^{(1111)}(\boldsymbol{\phi})}{\omega_L^3}+(N+1)\frac{V_k^{(gghh)}(\boldsymbol{\phi})}{\omega_T^3}\right\}\Bigg] \quad \text{for} \quad h \neq g, h \neq 1. \tag{D6}$$

Following the expansion introduced in Ref. [14], at the leading iteration the propagators appearing in the loop integrals generated by the right-hand side of the Wetterich equation are evaluated by setting $\Omega_k = Z_k = Z_{0,k}$. The flows of these three quantities are nevertheless obtained from different projections of the Wetterich equation. In particular, the boundary projection gives $\eta_{Z_0} \neq \eta_Z$. A higher iteration of the scheme in Ref. [14] would use the resulting distinct values of the renormalization functions to update the propagators inside the loop integrals.

Here, we work at the level of the leading iteration and find

$$\eta_{Z_0}^{(m)} = -\int_{\boldsymbol{q}} \frac{\partial_\kappa R}{2}\Bigg\{\frac{3U_k''(\rho)+12\rho U_k^{(3)}(\rho)+4\rho^2U_k^{(4)}(\rho)}{\omega_L^3}+(N-1)\frac{U_k''(\rho)+2\rho U_k^{(3)}(\rho)}{\omega_T^3} - 3\rho\left[\frac{[3U_k''(\rho)+2\rho U_k'''(\rho)]^2}{\omega_L^4}+(N-1)\frac{U_k''(\rho)^2}{\omega_T^4}\right]\Bigg\}, \tag{D7a}$$

$$\eta_{Z_0}^{(g)} = -\int_{\boldsymbol{q}} \frac{\partial_\kappa R}{2}\left\{\frac{U_k''(\rho)+2\rho U_k^{(3)}(\rho)}{\omega_L^3}+(N+1)\frac{U_k''(\rho)}{\omega_T^3}-4\rho U_k''(\rho)^2\frac{\left(\omega_L^4+2\omega_L^3\omega_T+2\omega_L\omega_T^3+\omega_T^4\right)}{(\omega_L+\omega_T)^2\omega_L^3\omega_T^3}\right\}, \tag{D7b}$$

where the integration over momenta has finally been reintroduced, as both R_k and $\omega_{i,k}$ depend on the modulus of $\boldsymbol{q}$.

2. Flow of Ω

Similarly, if we are interested in the flow of Ω_k, we find

$$-2\int_t \partial_\kappa\Omega\,\delta\tilde{\phi}_i\delta\tilde{\phi}_i = \frac{\partial_\kappa R}{2}\int_t \mathrm{tr}\left\{\delta^2_{\tilde{\phi}_i\tilde{\phi}_i}\mathbb{G}(t,t)\hat{\tau}_1\right\}, \tag{D8}$$

where the trace on the right-hand side is given by

$$\sum_{a,b=1}^{N}\int_{t',t''}\mathrm{tr}\left\{\left[\mathbb{G}_a(t,t'')\left(\delta_{\tilde{\phi}_j}\Gamma^{(2)}\right)_{ab}\mathbb{G}_b(t'',t')\left(\delta_{\tilde{\phi}_i}\Gamma^{(2)}\right)_{ba}\mathbb{G}_a(t',t)+\mathbb{G}_a(t,t')\left(\delta_{\tilde{\phi}_i}\Gamma^{(2)}\right)_{ab}\mathbb{G}_b(t',t'')\left(\delta_{\tilde{\phi}_j}\Gamma^{(2)}\right)_{ba}\mathbb{G}_a(t'',t)\right]\hat{\tau}_1\right\}, \tag{D9}$$

and the remaining trace is over the 2×2 matrix structure only. We can perform the latter and the two time integrals to obtain

$$\sum_{a,b=1}^{N}\left\{\frac{4\Omega_k^2}{Z_k}\frac{[2-e^{-(\omega_a+\omega_b)(t-t_0)/Z_k}]\,\omega_a+\omega_b}{\omega_a^2\omega_b(\omega_a+\omega_b)^2}+\gamma_k\mathcal{E}_1+\gamma_k^2\mathcal{E}_2\right\}V^{(abi)}(\boldsymbol{\phi})^2\delta\tilde{\phi}_i\delta\tilde{\phi}_i, \tag{D10}$$

where $\mathcal{E}_1$ and $\mathcal{E}_2$ denote terms that are exponentially suppressed in the variable $(t-t_0)$. More precisely, they are sums of several terms proportional to $e^{-\alpha(t-t_0)}$ with some $\alpha > 0$. We are going to ignore terms of this kind. On the other hand, the time dependence enters only through the latter, so we are effectively approximating Ω_k (and indeed the other renormalization functions as well as the potential) as time-independent quantities. As a by-product of this observation, it is expected that deviations from the fluctuation-dissipation theorem manifesting as differences in the flow of Z_k and Ω_k decay exponentially fast in time. We finally get

$$-\frac{\partial_\kappa\Omega_k}{\Omega_k} = \frac{\Omega_k}{Z_k}\sum_{a,b=1}^{N}V^{(abi)}(\boldsymbol{\phi})^2\int_{\boldsymbol{q}}\partial_\kappa R\frac{2\omega_a+\omega_b}{\omega_a^2\omega_b(\omega_a+\omega_b)^2}, \tag{D11}$$

which, upon choosing $i = g \neq 1$, leads to

$$\partial_\kappa\Omega_k = -\Omega_k V_k^{(1gg)2}\int_{\boldsymbol{q}}\partial_\kappa R_k\frac{\omega_L^2+4\omega_L\omega_T+\omega_T^2}{\omega_L^2\omega_T^2(\omega_L+\omega_T)^2}, \tag{D12}$$

where $V_k^{(111)} = \sqrt{2\rho}[3U_k''(\rho)+2\rho U_k'''(\rho)]$ and $V_k^{(1gg)} = \sqrt{2\rho}U_k''(\rho)$.

APPENDIX E: THRESHOLD FUNCTIONS

For the derivation of flow equations, we have defined the dimensionless variable $\tilde{y} \equiv q^\sigma/k^\sigma$ and then used

$$\int_{\boldsymbol{q}} \frac{\partial_\kappa R_k(q^\sigma)}{[K_k q^\sigma + R_k(q^\sigma) + K_k k^\sigma w]^{n+1}} = \frac{4v_d k^d}{(K_k k^\sigma)^n} \frac{2}{\sigma} \frac{L_n^{(d,\sigma)}(w)}{(n+\delta_{n,0})},$$

$$L_n^{(d,\sigma)}(w) := \frac{n+\delta_{n,0}}{2} \int_0^\infty d\tilde{y} \frac{\tilde{y}^{\frac{d}{\sigma}-1}\, s(\tilde{y})}{[p(\tilde{y})+w]^{n+1}}. \tag{E1}$$

The functions $L_n^{(d,\sigma)}(\cdot)$ are called threshold functions. We have used $\int_{\boldsymbol{q}} \equiv \int \frac{d^d q}{(2\pi)^d} = \frac{4v_d k^d}{\sigma} \int_0^\infty d\tilde{y}\, \tilde{y}^{\frac{d}{\sigma}-1}$. Moreover, we have introduced the dimensionless shape function $r(\tilde{y})$, defined by $R_k(q^\sigma) =: K_k q^\sigma r(\tilde{y})$, and the auxiliary quantities $s(\tilde{y})$ and $p(\tilde{y})$:

$$\partial_\kappa R_k(q^\sigma) =: K_k k^\sigma s(\tilde{y}) \Rightarrow s(\tilde{y}) = -\tilde{y}[\eta_K r(\tilde{y}) + \sigma \tilde{y} r'(\tilde{y})],$$
$$p(\tilde{y}) := \tilde{y}(1 + r(\tilde{y})). \tag{E2}$$

If we choose the flat cutoff (45),

$$r(\tilde{y}) = \frac{(1-\tilde{y})\,\vartheta(1-\tilde{y})}{\tilde{y}}, \quad s(\tilde{y}) = [\sigma - \eta_K(1-\tilde{y})]\vartheta(1-\tilde{y}),$$
$$p(\tilde{y}) = \tilde{y} + (1-\tilde{y})\,\vartheta(1-\tilde{y}) = 1, \text{ if } \tilde{y} < 1. \tag{E3}$$

Thus, the corresponding threshold functions are

$$L_n^{(d,\sigma)}(w) = \frac{\sigma^2}{2d}\left(1 - \frac{\eta_K}{d+\sigma}\right) \frac{n+\delta_{n,0}}{(1+w)^{n+1}}, \tag{E4}$$

which reduce to the well-known functions of the theory with momentum dependence $\sim q^2$ [85] in the limit $\sigma = 2$.

APPENDIX F: EXTRACTION OF THE SHORT-TIME BEHAVIOR

In general, we have to evaluate integrals of the shape

$$J := \int_{t_0}^\infty dt\, \chi(\Phi(t)) f(t-t_0) e^{-\varpi(t-t_0)}, \tag{F1}$$

where $\varpi \equiv 2\omega_k(q)/Z_k$, χ is a function of time through the fields $\phi, \tilde{\phi}$, and all our cases are covered by

$$f(t) = 1 + a\frac{\varpi t}{2} + b\left(\frac{\varpi t}{2}\right)^2 + c_{\tau_0}(t), \quad c_{\tau_0} = O\big(\tau_0^{-1}\big). \tag{F2}$$

Note that $c_{\tau_0}(0) = 0$, so that the property $f(0) = 1$ is guaranteed. Moreover, $c_{\tau_0}(t)$ is also at most $O(t^2)$. Omitting the dependence on all parameters but t, we define

$$g(t) \equiv \chi(\Phi(t)) f(t - t_0). \tag{F3}$$

For any well-behaved function $g(t)$ that admits a Taylor expansion around $t = t_0$ and any $C > 0$ satisfies

$$\int_{t_0}^\infty dt\, g(t) e^{-C(t-t_0)} = \sum_{n=0}^\infty \frac{1}{C^{n+1}} g^{(n)}(t_0). \tag{F4}$$

Thus, using the identity (F4), we get

$$J = \sum_{n=0}^\infty \frac{1}{\varpi^{n+1}} \partial_t^n g(t)|_{t=t_0}. \tag{F5}$$

Next, the general Leibniz rule reads

$$\partial_t^n g(t) = \sum_{k=0}^n \binom{n}{k} \partial_t^{n-k} \chi(\Phi(t))\, \partial_t^k f(t-t_0), \tag{F6}$$

for the nth derivative of $g(t)$. This implies that for $n \geqslant 2$,

$$\partial_t^n g(t)|_{t=t_0} = \Bigg[\frac{n(n-1)}{2} \partial_t^{n-2} \chi(\Phi(t))\, \partial_t^2 f(t-t_0) + n\partial_t^{n-1} \chi(\Phi(t))\, \partial_t f(t-t_0) + \partial_t^n \chi(\Phi(t))\Bigg]\Bigg|_{t=t_0}, \tag{F7}$$

because $\partial_t^k f(t-t_0)|_{t=t_0} = 0$ for all $k > 2$. One concludes

$$J = \chi(\Phi(t_0))\left[\frac{1}{\varpi} + \frac{f'(0)}{\varpi^2} + \frac{f''(0)}{\varpi^3}\right] + \cdots = \frac{1 + a/2 + b/2}{\varpi} \chi(\Phi(t_0)) + \cdots, \tag{F8}$$

where the dots denote all terms with at least one time derivative of the fields and are therefore negligible for the flow of $Z_{0,k}$ studied in Appendix D. We have also left out the $O(\tau_0^{-1})$ terms, which evaluate to zero at the fixed point due to their dimensionality.

[1] A. Campa, T. Dauxois, and S. Ruffo, Statistical mechanics and dynamics of solvable models with long-range interactions, Phys. Rep. **480**, 57 (2009).

[2] N. Defenu, T. Donner, T. Macrì, G. Pagano, S. Ruffo, and A. Trombettoni, Long-range interacting quantum systems, Rev. Mod. Phys. **95**, 035002 (2023).

[3] N. Defenu, A. Lerose, and S. Pappalardi, Out-of-equilibrium dynamics of quantum many-body systems with long-range interactions, Phys. Rep. **1074**, 1 (2024).

[4] A. Browaeys and T. Lahaye, Many-body physics with individually controlled Rydberg atoms, Nat. Phys. **16**, 132 (2020).

[5] J. W. Britton, B. C. Sawyer, A. C. Keith, C.-C. J. Wang, J. K. Freericks, H. Uys, M. J. Biercuk, and J. J. Bollinger, Engineered two-dimensional Ising interactions in a trapped-ion quantum simulator with hundreds of spins, Nature (London) **484**, 489 (2012).

[6] T. Lahaye, C. Menotti, L. Santos, M. Lewenstein, and T. Pfau, The physics of dipolar bosonic quantum gases, Rep. Prog. Phys. **72**, 126401 (2009).

[7] H. Ritsch, P. Domokos, F. Brennecke, and T. Esslinger, Cold atoms in cavity-generated dynamical optical potentials, Rev. Mod. Phys. **85**, 553 (2013).

[8] P. C. Hohenberg and B. I. Halperin, Theory of dynamic critical phenomena, Rev. Mod. Phys. **49**, 435 (1977).

[9] H. Christiansen, S. Majumder, M. Henkel, and W. Janke, Aging in the long-range Ising model, Phys. Rev. Lett. **125**, 180601 (2020).

[10] H. K. Janssen, B. Schaub, and B. Schmittmann, New universal short-time scaling behaviour of critical relaxation processes, Z. Phys. B **73**, 539 (1989).

[11] H. K. Janssen, On the renormalized field theory of nonlinear critical relaxation, in *From Phase Transitions To Chaos: Topics in Modern Statistical Physics*, edited by G. Gyoergyi, I. Kondor, L. Sasvari, and T. Tel (World Scientific, Singapore, 1992), pp. 68–91.

[12] Y. Chen, S. Guo, Z. Li, S. Marculescu, and L. Schülke, The short-time critical behaviour of the Ginzburg-Landau model with long-range interaction, Eur. Phys. J. B **18**, 289 (2000).

[13] P. Calabrese and A. Gambassi, Ageing properties of critical systems, J. Phys. A **38**, R133 (2005).

[14] F. Ihssen, V. Pagni, J. Marino, S. Diehl, and N. Defenu, Nonperturbative treatment of a quenched Langevin field theory, Phys. Rev. B **112**, 024306 (2025).

[15] Edited by M. Henkel, M. Pleimling, and R. Sanctuary, *Ageing and the Glass Transition* (Springer, Berlin, Heidelberg, 2007), Vol. 716.

[16] M. Henkel and M. Pleimling, *Non-Equilibrium Phase Transitions: Volume 2: Ageing and Dynamical Scaling Far From Equilibrium* (Springer, Dordrecht, 2011), Vol. 2.

[17] L. F. Cugliandolo, Dynamics of glassy systems, arXiv:cond-mat/0210312.

[18] K. Uzelac, Z. Glumac, and O.-S. Barišić, Short-time dynamics in the 1D long-range Potts model, Eur. Phys. J. B **63**, 101 (2008).

[19] D. E. Rodriguez, M. A. Bab, and E. V. Albano, Study of the nonequilibrium critical quenching and the annealing dynamics for the long-range Ising model in one dimension, J. Stat. Mech. (2011) P09007.

[20] R. A. Baños, L. A. Fernandez, V. Martin-Mayor, and A. P. Young, Correspondence between long-range and short-range spin glasses, Phys. Rev. B **86**, 134416 (2012).

[21] M. C. Angelini, G. Parisi, and F. Ricci-Tersenghi, Relations between short-range and long-range Ising models, Phys. Rev. E **89**, 062120 (2014).

[22] N. Defenu, A. Trombettoni, and A. Codello, Fixed-point structure and effective fractional dimensionality for O(N) models with long-range interactions, Phys. Rev. E **92**, 052113 (2015).

[23] N. Defenu, A. Trombettoni, and S. Ruffo, Criticality and phase diagram of quantum long-range O(N) models, Phys. Rev. B **96**, 104432 (2017).

[24] A. Solfanelli and N. Defenu, Universality in long-range interacting systems: The effective dimension approach, Phys. Rev. E **110**, 044121 (2024).

[25] M. Campisi and R. Fazio, The power of a critical heat engine, Nat. Commun. **7**, 11895 (2016).

[26] J. Sak, Recursion relations and fixed points for ferromagnets with long-range interactions, Phys. Rev. B **8**, 281 (1973).

[27] M. Picco, Critical behavior of the Ising model with long range interactions, arXiv:1207.1018.

[28] T. Blanchard, M. Picco, and M. Rajabpour, Influence of long-range interactions on the critical behavior of the Ising model, Europhys. Lett. **101**, 56003 (2013).

[29] E. Luijten and H. W. Blöte, Boundary between long-range and short-range critical behavior in systems with algebraic interactions, Phys. Rev. Lett. **89**, 025703 (2002).

[30] E. Brezin, G. Parisi, and F. Ricci-Tersenghi, The crossover region between long-range and short-range interactions for the critical exponents, J. Stat. Phys. **157**, 855 (2014).

[31] C. Behan, L. Rastelli, S. Rychkov, and B. Zan, Long-range critical exponents near the short-range crossover, Phys. Rev. Lett. **118**, 241601 (2017).

[32] C. Behan, L. Rastelli, S. Rychkov, and B. Zan, A scaling theory for the long-range to short-range crossover and an infrared duality, J. Phys. A: Math. Theor. **50**, 354002 (2017).

[33] D. Benedetti, E. Lauria, D. Mazáč, and P. van Vliet, One-dimensional Ising model with $1/r^{1.99}$ interaction, Phys. Rev. Lett. **134**, 201602 (2025).

[34] V. Pagni, G. Giachetti, A. Trombettoni, and N. Defenu, One-dimensional long-range ising model: Two almost equivalent approximations, Phys. Rev. B **113**, 014406 (2026).

[35] J. Cardy, *Scaling and Renormalization in Statistical Physics* (Cambridge University Press, Cambridge, 1996), Vol. 5.

[36] U. C. Täuber, *Critical Dynamics: A Field Theory Approach to Equilibrium and Non-Equilibrium Scaling Behavior* (Cambridge University Press, Cambridge, 2014).

[37] P. C. Martin, E. D. Siggia, and H. A. Rose, Statistical dynamics of classical systems, Phys. Rev. A **8**, 423 (1973).

[38] H.-K. Janssen, On a Lagrangean for classical field dynamics and renormalization group calculations of dynamical critical properties, Z. Phys. B **23**, 377 (1976).

[39] C. De Dominicis, Dynamics as a substitute for replicas in systems with quenched random impurities, Phys. Rev. B **18**, 4913 (1978).

[40] J. C. Halimeh and M. F. Maghrebi, Quantum aging and dynamical universality in the long-range $O(N \to \infty)$ model, Phys. Rev. E **103**, 052142 (2021).

[41] M. Moshe and J. Zinn-Justin, Quantum field theory in the large N limit: A review, Phys. Rep. **385**, 69 (2003).

[42] J. Cardy, *Finite-Size Scaling* (Elsevier, Amsterdam, 2012).

[43] J. Honkonen and M. Y. Nalimov, Crossover between field theories with short-range and long-range exchange or correlations, J. Phys. A: Math. Gen. **22**, 751 (1989).

[44] J. Honkonen, Critical behaviour of the long-range $(\varphi^2)^2$ model in the short-range limit, J. Phys. A: Math. Gen. **23**, 825 (1990).

[45] A. Codello and G. D'Odorico, O(N)-universality classes and the Mermin-Wagner theorem, Phys. Rev. Lett. **110**, 141601 (2013).

[46] N. Tetradis and C. Wetterich, Critical exponents from the effective average action, Nucl. Phys. B **422**, 541 (1994).

[47] N. Dupuis, L. Canet, A. Eichhorn, W. Metzner, J. M. Pawlowski, M. Tissier, and N. Wschebor, The nonperturbative functional renormalization group and its applications, Phys. Rep. **910**, 1 (2021).

[48] N. Defenu, A. Codello, S. Ruffo, and A. Trombettoni, Criticality of spin systems with weak long-range interactions, J. Phys. A: Math. Theor. **53**, 143001 (2020).

[49] A. Chiocchetta, A. Gambassi, S. Diehl, and J. Marino, Universal short-time dynamics: Boundary functional renormalization group for a temperature quench, Phys. Rev. B **94**, 174301 (2016).

[50] C. Wetterich, Exact evolution equation for the effective potential, Phys. Lett. B **301**, 90 (1993).
[51] L. Canet and H. Chaté, A non-perturbative approach to critical dynamics, J. Phys. A: Math. Theor. **40**, 1937 (2007).
[52] L. Canet, H. Chaté, and B. Delamotte, General framework of the non-perturbative renormalization group for non-equilibrium steady states, J. Phys. A **44**, 495001 (2011).
[53] C. Duclut and B. Delamotte, Frequency regulators for the nonperturbative renormalization group: A general study and the model A as a benchmark, Phys. Rev. E **95**, 012107 (2017).
[54] D. F. Litim, Optimisation of the exact renormalisation group, Phys. Lett. B **486**, 92 (2000).
[55] D. F. Litim, Optimized renormalization group flows, Phys. Rev. D **64**, 105007 (2001).
[56] Y. Tomita, Monte Carlo study of one-dimensional Ising models with long-range interactions, J. Phys. Soc. Jpn. **78**, 014002 (2009).
[57] R. Aiudi, R. Burioni, and A. Vezzani, Critical dynamics of long-range models on dynamical lévy lattices, Phys. Rev. B **107**, 224204 (2023).
[58] P. Grassberger, Damage spreading and critical exponents for "model A" Ising dynamics, Physica A **214**, 547 (1995).
[59] M. Nightingale and H. Blöte, Monte Carlo computation of correlation times of independent relaxation modes at criticality, Phys. Rev. B **62**, 1089 (2000).
[60] M. Hasenbusch, Dynamic critical exponent z of the three-dimensional Ising universality class: Monte Carlo simulations of the improved blume-capel model, Phys. Rev. E **101**, 022126 (2020).
[61] C.-H. Chang, V. Dommes, R. S. Erramilli, A. Homrich, P. Kravchuk, A. Liu, M. S. Mitchell, D. Poland, and D. Simmons-Duffin, Bootstrapping the 3D Ising stress tensor, J. High Energy Phys. 03 (2025) 136.
[62] P. Pietzonka and U. Seifert, Universal trade-off between power, efficiency, and constancy in steady-state heat engines, Phys. Rev. Lett. **120**, 190602 (2018).
[63] R. Masaoka, T. Soejima, and H. Watanabe, Rigorous lower bound of the dynamical critical exponent of the Ising model, J. Stat. Phys. **192**, 76 (2025).
[64] Y. Chen, Short-time dynamics of a random Ising model with long-range interaction, Phys. Rev. E **66**, 037104 (2002).
[65] Y. Deng, T. M. Garoni, and A. D. Sokal, Critical speeding-up in the local dynamics of the random-cluster model, Phys. Rev. Lett. **98**, 230602 (2007).
[66] Y. Deng, T. M. Garoni, and A. D. Sokal, Dynamic critical behavior of the worm algorithm for the Ising model, Phys. Rev. Lett. **99**, 110601 (2007).
[67] E. M. Elçi and M. Weigel, Efficient simulation of the random-cluster model, Phys. Rev. E **88**, 033303 (2013).
[68] B. Zappoli, D. Bailly, Y. Garrabos, B. Le Neindre, P. Guenoun, and D. Beysens, Anomalous heat transport by the piston effect in supercritical fluids under zero gravity, Phys. Rev. A **41**, 2264 (1990).
[69] H. Boukari, M. E. Briggs, J. Shaumeyer, and R. W. Gammon, Critical speeding up observed, Phys. Rev. Lett. **65**, 2654 (1990).
[70] C. P. Grams, M. Valldor, M. Garst, and J. Hemberger, Critical speeding-up in the magnetoelectric response of spin-ice near its monopole liquid–gas transition, Nat. Commun. **5**, 4853 (2014).
[71] M. Tavora, A. Rosch, and A. Mitra, Quench dynamics of one-dimensional interacting bosons in a disordered potential: Elastic dephasing and critical speeding-up of thermalization, Phys. Rev. Lett. **113**, 010601 (2014).
[72] M. Sarkar, N. Defenu, and T. Enss, Long range to short range crossover in one dimension, arXiv:2507.08092.
[73] A. Solfanelli, G. Giachetti, M. Campisi, S. Ruffo, and N. Defenu, Quantum heat engine with long-range advantages, New J. Phys. **25**, 033030 (2023).
[74] A. Solfanelli and N. Defenu, Universal work statistics in long-range interacting quantum systems, Phys. Rev. Lett. **134**, 030402 (2025).
[75] V. Holubec and A. Ryabov, Work and power fluctuations in a critical heat engine, Phys. Rev. E **96**, 030102 (2017).
[76] N. D. Mermin and H. Wagner, Absence of ferromagnetism or antiferromagnetism in one- or two-dimensional isotropic Heisenberg models, Phys. Rev. Lett. **17**, 1133 (1966).
[77] We note that integrating the fixed-point equation for large N and $\sigma \to 2$ becomes numerically challenging.
[78] A. Codello, N. Defenu, and G. D'Odorico, Critical exponents of O(N) models in fractional dimensions, Phys. Rev. D **91**, 105003 (2015).
[79] M. Henkel, Physical ageing from generalised time-translation-invariance, Nucl. Phys. B **1017**, 116968 (2025).
[80] L. Moueddene and M. Henkel, Short-time dynamics in phase-ordering kinetics, Int. J. Theor. Phys. **65**, 92 (2026).
[81] A. Chiocchetta, A. Gambassi, S. Diehl, and J. Marino, Dynamical crossovers in prethermal critical states, Phys. Rev. Lett. **118**, 135701 (2017).
[82] G. De Polsi, I. Balog, M. Tissier, and N. Wschebor, Precision calculation of critical exponents in the O(N) universality classes with the nonperturbative renormalization group, Phys. Rev. E **101**, 042113 (2020).
[83] B. Sciolla and G. Biroli, Quantum quenches, dynamical transitions, and off-equilibrium quantum criticality, Phys. Rev. B **88**, 201110 (2013).
[84] G. Bighin, T. Enss, and N. Defenu, Universal scaling in real dimension, Nat. Commun. **15**, 4207 (2024).
[85] J. Berges, N. Tetradis, and C. Wetterich, Non-perturbative renormalization flow in quantum field theory and statistical physics, Phys. Rep. **363**, 223 (2002).